Modeling and simulation of alkali-activated materials (AAMs)
A critical review

Zuo, Yibing; Chen, Yun; Liu, Chen; Gan, Yidong; Göbel, Luise; Ye, Guang; Provis, John L.

DOI
10.1016/j.cemconres.2024.107769

Publication date
2024

Document Version
Final published version

Published in
Cement and Concrete Research

Cement and Concrete Research 189 (2025) 107769

Contents lists available at ScienceDirect

Cement and Concrete Research

journal homepage: www.elsevier.com/locate/cemconres

Modeling and simulation of alkali-activated materials (AAMs): A critical review

Yibing Zuo [a,*], Yun Chen [b], Chen Liu [b], Yidong Gan [a], Luise Göbel [c], Guang Ye [b], John L. Provis [d]

[a] School of Civil Engineering and Hydraulic, Huazhong University of Science and Technology, Wuhan 430074, China
[b] Faculty of Civil Engineering and Geosciences, Delft University of Technology, Stevinweg 1, 2628 CN Delft, the Netherlands
[c] Chair of Mechanics of Engineering, Materials, Bauhaus-Universität Weimar, Coudraystraße 11A, Weimar 99423, Germany
[d] PSI Center for Nuclear Engineering and Sciences, Paul Scherrer Institut, Forschungsstrasse 111, 5232 Villigen PSI, Switzerland

ARTICLE INFO

Keywords:
Alkali-activated material
Atomistic simulation
Thermodynamics
Microstructure
Multi-scale modeling

ABSTRACT

Alkali-activated materials (AAMs) are a class of potentially eco-friendly construction materials that can contribute to reduce the environmental impact of the construction sector by offering an alternative to Portland cement (PC). With the rapid development of both computational capabilities and theoretical insights into alkali-activation reaction processes, there has been a surge in research activities worldwide, leading to a growing demand for computational methods that can describe different characteristics of AAMs. This review summarizes the collective efforts made in the past two decades on this topic, and highlights the most relevant results and advances in the aspects of atomistic simulation, thermodynamic modeling, microstructure/−based simulation, and multi-scale modeling. The gaps and challenges in current numerical research on AAMs are pointed out and discussed in comparison with PC-based materials. This review aims to provide a critical overview of the state-of-the-art in modeling and simulating AAMs, while also outlining potential avenues for future development.

1. Introduction

Alkali-activated materials (AAMs) have gained popularity as low-carbon construction materials due to their ability to significantly reduce the carbon dioxide footprint and improve concrete production sustainability. Besides the opportunity for significantly reducing environmental impact, AAMs also have the potential to achieve comparable or even superior performance properties to PC-based materials [1–4]. Therefore, AAMs show promising potential for use in the construction materials industry [5–7].

Numerical models are useful vehicles for comprehending and describing the engineering properties of construction materials, providing us with an important numerical study route in addition to experimentation [8,9]. Interest in the modeling and simulation of PC and AAMs has increased continuously and rapidly, parallel to the fast evolution of computational power and technology. The great driving-force for modeling and simulation of AAMs results from their promising sustainability as well as diversity and complexity. While many numerical models have been well developed and widely used in the studies of PC-based materials, such as the hydration and microstructure simulation models HYMOSTRUC [10] and CEMHYD3D [11], they are not immediately applicable to AAMs due to intrinsic differences in at least three aspects:

- *Raw materials.* Precursors and alkaline activators are two raw material components of AAMs that evidently differ from those of PC. Precursors of AAMs stem from a wide variety of local sources and differ greatly in chemical and physical properties, such as chemical composition and reactivity on the one hand, and particle size distribution and specific surface area on the other hand [12,13]. In addition to the precursor, the alkaline activators used in AAMs also exhibit great diversity, illustrated by the type of alkali ion (sodium or potassium) as well as the alkaline salts, such as sodium sulfate and sodium carbonate, etc. [13,14]. In comparison with PC that shows relatively well-defined clinker mineral compositions and corresponding explicitly defined hydration reactions, the mineral composition and reactivity of the amorphous phases in the precursor are not always clearly known, and the reaction of multiple amorphous phases with the alkaline activator (when present, e.g. in fly ash) is often described in bulk rather than phase-specific terms.
- *Reaction products*. The reaction products of AAMs exhibit a wide range of diversity and differ significantly from those of PC-based

* Corresponding author.
E-mail address: zuoyibing@hust.edu.cn (Y. Zuo).

https://doi.org/10.1016/j.cemconres.2024.107769
Received 5 June 2024; Received in revised form 28 November 2024; Accepted 5 December 2024
Available online 10 December 2024

materials, as illustrated in Table 1. According to the calcium content of the amorphous phase in the precursor and the type of the primary reaction product, AAMs are typically categorized into alkali-activated high-Ca, low-Ca and medium-Ca systems [13,15,16]. The alkali-activated high-Ca system is represented by alkali-activated slag, which produces an alkali calcium-aluminosilicate hydrate (C-(N-)A-S-H) type gel as its primary reaction product. The alkali-activated low-Ca system is represented by alkali-activated fly ash or metakaolin, which produces a three-dimensional hydrous alkali-aluminosilicate (N-A-S-H) type gel as its primary reaction product. The alkali-activated medium-Ca system is represented by a blend of alkali-activated slag and fly ash, whose primary reaction products are co-existing C-(N-)A-S-H and N-A-S-H gels. In addition to the primary reaction product, the secondary reaction products of AAMs are also diverse, depending on not only the type and composition of the precursor but also on the type of alkaline activator and curing conditions [17,18].

- *Pore solution chemistry*. Due to the presence of the alkaline activator, the pore solution of AAMs can have a higher ionic strength than that of PC-based materials, with particularly high concentrations of sodium and hydroxide ions, and also silicate ions at early age before they are incorporated into binding phases [20–22]. The complex pore solution composition influences the thermodynamics [23,24], kinetics [25,26] and durability [27,28] of AAMs. Therefore, it is important and necessary to carefully consider the chemistry of the pore solution in modeling and simulation of AAMs, even though it is often overlooked in the modeling and simulation of PC-based materials [10,11].

It is important to note that the raw materials, reaction products, and pore solution chemistry of AAMs are not independent of each other, but rather, they all strongly influence each other. This adds to the complexity of modeling and simulating AAMs. Although the intrinsic diversity of AAMs motivates increasing research efforts in modeling and simulating them, it also presents challenges. These challenges are especially apparent when compared to the advanced computational means available for PC-based materials. To gain a clear knowledge of these challenges and gaps, a comprehensive review of the state-of-art in modeling and simulation of AAMs is necessary. This is the core aim of the current paper.

Fig. 1 classifies the types of numerical studies that have been carried out for AAMs. From the multi-scale viewpoint, numerical studies of AAMs can be classified into: (i) atomistic simulations of C-(N-)A-S-H and N-A-S-H gels, (ii) thermodynamic modeling of reaction products assemblage, (iii) simulation of microstructure formation and microstructure-based modeling of properties, and (iv) multiscale modeling of *meso* and macro properties of AAMs. It should be noted that although multiscale modeling has been usually used to study meso/macro properties of AAM mortar/concrete, it does not mean that it could not be applied to study the properties of AAMs at micro-scale and even below. In addition to the scale-dependent numerical studies, kinetic modeling is also applied to analyze the material evolution of AAMs over time. Since the simplified empirical kinetic models are not within our scope, the present review aims to highlight the most significant results and advancements in the first four aspects over the past two decades. More information on the kinetic modeling could be referred to [29]. Since this review is more focused on the microstructure-based multiscale modeling, empirical or semi-empirical models for physical properties of AAM mortar/concrete are not covered, although there are plenty of studies on that in the literature [30–32]. The present review shall provide a reference for evaluating recent advances in modeling and simulation approaches, and further perspectives for future computer-based investigations and developments regarding AAMs.

Table 1
Reaction products of AAMs and PC-based materials [19].

Reaction products	OPC	AAMs	
		Alkali-activated slag	Alkali-activated fly ash
Primary	C-S-H	C-(N-)A-S-H	N-A-S-H
Secondary	CH, AFm, AFt	Hydrotalcite, potentially AFm (e.g. C_4AH_{13}, C_2ASH_8, C_4AcH_{11}, C_4AcH_{12}) depending on activator, sometimes N-A-S-H	Hydroxysodalite, zeolites including Na-chabazite, faujasite, zeolite P ($N_3A_3S_{14}H_{15}$), zeolite LTA, and others

Notation/abbreviations: C = CaO, S = SiO_2, A = Al_2O_3, N = Na_2O, H = H_2O, c = CO_2, AFm = monosulfate aluminate hydrate, AFt = ettringite

2. Atomistic simulation of C-(N-)A-S-H and N-A-S-H gels

The dominant reaction product phase in AAMs is C-(N-)A-S-H gel or N-A-S-H gel, depending on the Ca content in the system [13]. The C-(N-)A-S-H and N-A-S-H gels are the unique reaction products in AAMs, whose composition and structure differ from the calcium silicate hydrate (C-S-H) type gel in PC-based materials, and notably they play a crucial role in determining the mechanical properties and long-term durability of AAMs. In parallel with physical experiments, atomistic simulation tools such as density functional theory (DFT), molecular dynamic (MD) simulation and Grand Canonical Monte Carlo (GCMC) simulation can also provide valuable insights into the atomistic structure, intrinsic mechanical properties and transport-related issues of these gels.

2.1. Atomistic simulation of C-(N-)A-S-H gel

Compared to C-S-H gels in PC-based systems, the C-(N-)A-S-H gel in high-Ca AAMs shows lower Ca/Si ratios (0.6–1.2) and higher Al/Si ratios (0.1–0.3) [33–35]. This diverging chemical composition entails also different atomistic structures and local ordering [36–38], mechanical properties [39–42] and durability performance from C-S-H gels [43–46].

As a consequence of the lower Ca/Si ratios, the gel in high-Ca AAMs systems exhibits a longer mean chain length (MCL) than that in PC-based systems [47,48]. Moreover, the presence of Q^3 and Q^4 units has been detected in both experimental and simulation studies [36,47]. This indicates the formation of both crosslinked C-(N-)A-S-H gels (containing Q^3 sites) and also a N-A-S-H gel component (Q^4 sites) in high-Ca AAMs [36]. It was reported that the Al—Si substitution predominantly occurs in the bridge site of silica chains, which facilitates cross-linking between adjacent silicate layers [37,49]. Churakov and Labbez [49] further claimed that the chemical affinity of aluminum to C-S-H is influenced by both electrostatic interactions and the aqueous molar ratio of $Al(OH)_4^-$ to $Si(OH)_3O^-$. The strongest Al affinity is noted at a pH around 11.5, aligning with the maximum concentration of $SiO(OH)^-$ surface species. It is interesting to note that the Ca—Al substitution was also confirmed by experimental methods [50], which have been successfully reproduced by atomistic simulation [37]. The results demonstrate that Al can exhibit penta- or octahedral coordination with surrounding water molecules, which promotes the lengthening of silica chains and enhances the cross-linkage between layers. Furthermore, the structure of C-(N-)A-S-H gel can also be altered by alkali metal ions like Na^+ and K^+ ions. The addition of alkali metal ions leads to a decrease in basal spacing, mean silicate chain lengths, and the degree of silicate polymerization, as indicated by DFT results [51]. According to experimental and simulation works, representative models of (A) cross-linked and (B) non-cross-linked C-(N-)A-S-H gels in AAM systems were proposed by Myers [33,52], as depicted in Fig. 2. Those structural descriptions have opened further opportunities for detailed analysis and simulation of complex chain-structured silicates that are relevant to higher-calcium AAM binders [39].

Wan et al. [40] investigated the mechanical performance of C-A-S-H gel in alkali-activated slag. Molecular models of C-A-S-H gel with different Al/Ca ratios were constructed by introducing the Al^{3+} ions into

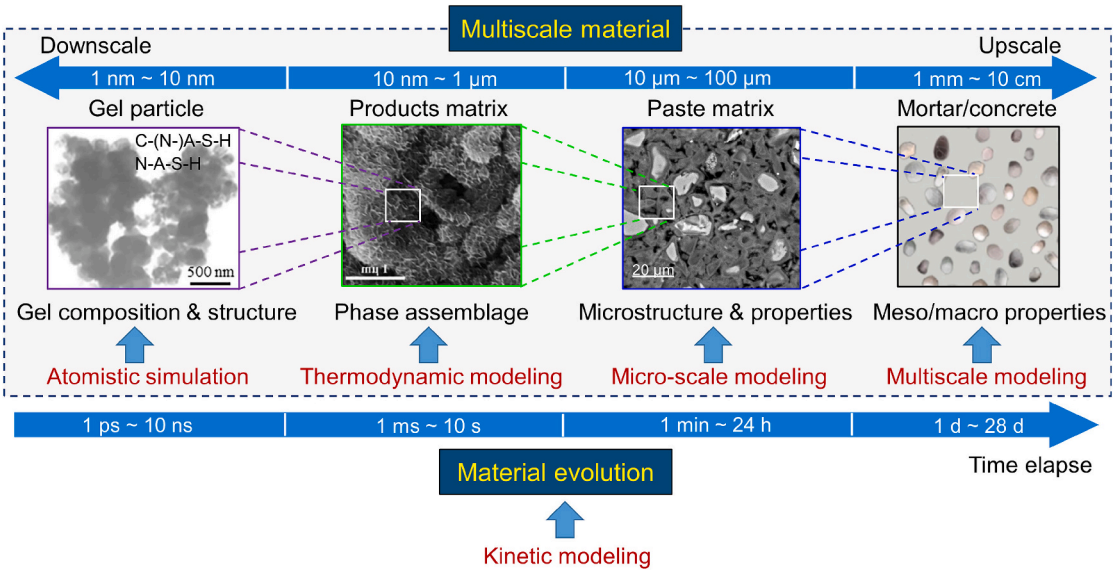

Fig. 1. Modeling and simulation of AAMs on different length and time scales.

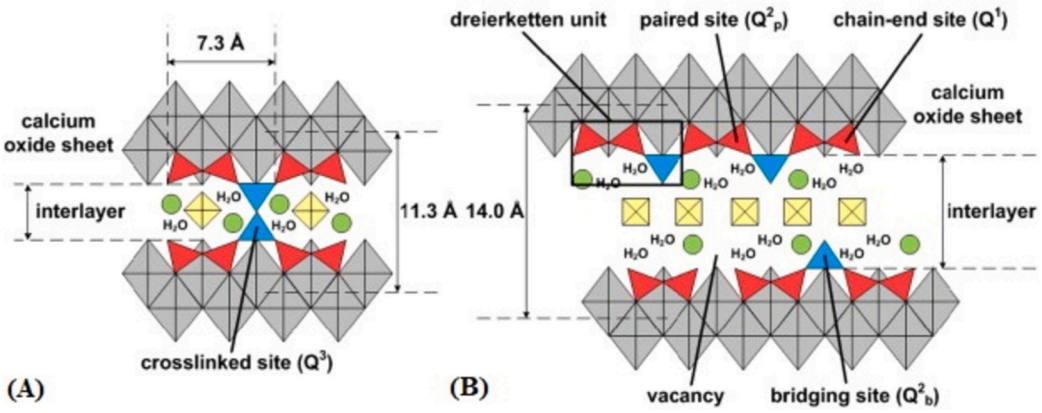

Fig. 2. Schematic diagrams of the nanostructures of (A) cross-linked and (B) non-cross-linked C-A-S-H gels with finite chain length [52]. The Ca species in the Ca—O sheet are represented by grey diamonds, while the red and blue triangles correspond to the aluminosilicate units in paired and bridging sites. The green circles and yellow squares are assigned to positively charged species, such as H^+, Ca^{2+}, or alkali ions like K^+ or Na^+, which neutralize the structure as a whole. (For interpretation of the references to colour in this figure legend, the reader is referred to the web version of this article.)

the interlayer region of C-S-H, as shown in Fig. 3(A). The uniaxial tension simulation results indicated that at an Al/Ca ratio of 0.08, the cracks generally initiate in the interlayer region. This area is abundant in fragile hydrogen bonds and Ca-O_w connections, potentially leading to the brittle failure of C-A-S-H gel. Additionally, at a high Al/Ca ratio, the branched Al-O-Si structures can bridge neighboring calcium silicate sheets, strengthening the weak interlayer region. During the tensile fracture process, aluminate atoms can reorganize to resist tensile loading and slow down the propagation of cracks, which is beneficial for the enhancement of the mechanical properties of C-A-S-H gel, as shown in Fig. 3 (B) and (C). Subsequently, the same research group conducted further atomistic simulations on C-A-S-H gels and found that the gels with extended Al—Si chains exhibit desirable loading resistance and cohesive strength [39,41]. Interestingly, the mechanical behavior of the C-A-S-H gel is associated with the depolymerization of silicate-aluminate chains and the hydrolysis of interlayer water molecules during the tensile failure process. Zhang et al. [42] explored the adhesion properties between polyvinyl alcohol (PVA) fibers and C-(N-)A-S-H gel by MD. They discovered that the adhesion between PVA fiber and the gel with high Ca/(Si + Al) ratios (>1) primarily results from the electrostatic interaction between the hydroxyl group in PVA and the alkali metal ions in C-(N-)A-S-H gel. Conversely, when the Ca/(Si + Al) ratios decreases to <1, the adhesion is mainly attributed to hydrogen bonding between PVA and C-(N-)A-S-H gels.

With regard to durability issues, several works have investigated chloride penetration and sulfate attack on C-(A-)S-H gels. It was reported that Al—Si substitution can enhance the reactivity of bridging oxygen sites in Si-O-Al, thereby increasing the hydrophilicity of C-A-S-H gels [39,43,44]. This substitution results in a greater negative charge increment of oxygen atoms in the gel at the C-A-S-H interface, leading to a more significant polarization of the dipole moment of water molecules on the surface. Consequently, it reinforces the interfacial hydrogen bonds and prolongs the residence time of water around the aluminate sites [43]. Al—Si substitution provides additional charge on the oxygen sites that can associate with Na ions, forming more stable Na-O_S bonds that greatly immobilize the cations, e.g. during the transport of NaCl in the gel pores (as depicted in Fig. 4). The diffusion coefficient of Na^+ restricted within the nanometer-sized pores was found to be reduced by half in [44]. Additionally, the inner-sphere adsorption of Na^+ on the C-A-S-H surface is conducive to the secondary outer-sphere adsorption of Cl^- ions through formation of Na—Cl ionic pairs [43].

Researchers have also carried out atomistic simulations to explore

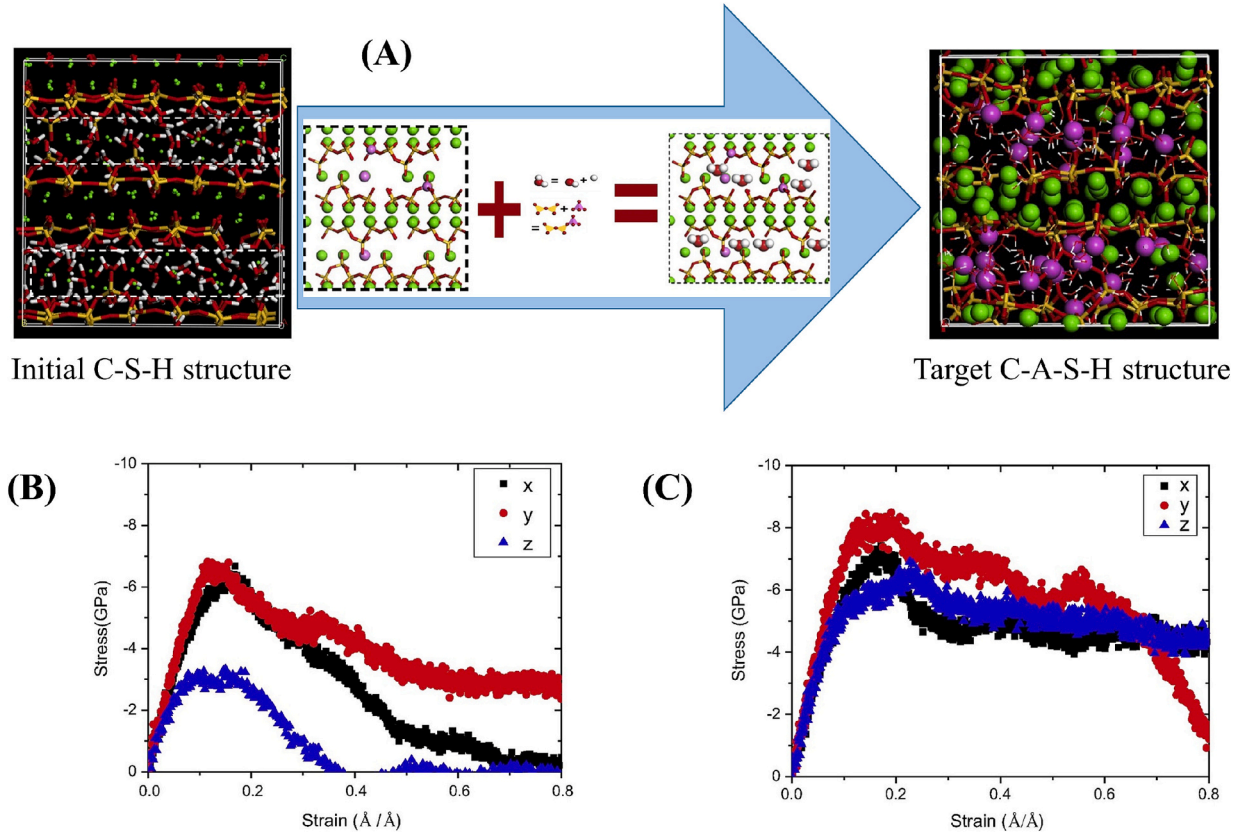

Fig. 3. (A) Schematic illustration for the C-A-S-H gel model construction procedure; (B) Stress-strain relation along x, y and z directions for the C-A-S-H gel with Al/Ca = 0 and (C) Al/Ca = 0.38 [40].

the resistance of C-(A-)S-H gels to sulfate attack. Liu et al. [45] investigated the effect of pH on the gel structure subjected to sulfate attack by using coupled experimental techniques and atomistic simulation. Both the experimental and simulation results showed that the interlayered Ca can become debonded under sulfate attack, which promotes the formation of oligomers in situ and increases the MCL of the C-S-H. Ding et al. [46] reported that sulfate attack can also cause the dealumination of C-A-S-H gels. Their molecular dynamic simulation results show that the interlayered Ca can be extracted by sulfate ions through the process of diffusion-absorption-dissociation, but the presence of Al can stabilize the gel structure and prevent the leaching of Ca.

So far, most atomistic simulation studies have focused on the C-(A-)S-H gel, which is the representative gel, with a low Al/Si ratio (0–0.05) and zero Na content, which is relevant to PC-SCMs blended systems. Atomistic simulation of the effect of higher Al/Si ratios (0.1–0.3) on the mechanical properties and durability of gels in high-Ca AAMs systems are less extensive and much of the behavior of these gels remains to be explored. It has been claimed that alkali metal ions, i.e. Na^+ and K^+, have weak binding in the interlayer of gels, which is considered to have limited impacts on the gel structure [53], although experimental studies have found significant differences in structural ordering with and without alkali cations [38]. However, in a recent publication [54], the structural change of gels in alkali-activated slag pastes after long-term water immersion was found. The leaching of pastes resulted in a marginal reduction in the Ca/Si ratio but a significant decrease in the Na/Si ratio, implying that the removal of sodium from the gels can alter the gel structure [55]. It is hoped that in future, the role of alkali ions in the C-(N-)A-S-H gels could be revealed in more detail using simulation methods. Improving the precision of gel construction is also tricky and essential.

2.2. Atomistic simulation of N-A-S-H gel

Atomistic simulation of N-A-S-H gel has been performed using MD simulation in several published works. GCMC simulation and DFT are also used in a few studies, but are limited by slow convergence or high computational cost [56]. Recent studies on the atomistic simulation of the N-A-S-H gel mainly focus on the reaction of its formation [57–59], nano-structural characterization [58,60–63], mechanical properties [64–67] and durability-related issues [68–73].

N-A-S-H gel forms as a result of the alkaline activation of aluminosilicate precursors, but only a few MD studies are devoted to simulating the alkali-activation reaction at the atomic scale. Although the geopolymerization process was modeled through the reaction among silicate and aluminate monomers in [57,58], the dissolution of precursors during the alkali-activation reaction was not considered. Hou et al. [59] modeled the reaction between metakaolin and sodium hydroxide through MD simulation. However, only silicates were dissolved from metakaolin, while aluminates were found stable during the reaction. Overall, the dissolution behavior of precursor and geopolymerization have been investigated at the molecular scale, respectively, while atomic simulation of the entire alkali-activation reaction, from the dissolution of precursor to the formation of N-A-S-H gel, needs to be further studied.

One commonly focused concern in atomic simulation of N-A-S-H gel is its nano-structural characteristics. N-A-S-H gel is generally considered as a 3D network of cross-linked Si and Al tetrahedral, as shown in Fig. 5. Penta-coordinate Al, previously believed to exist only in the precursor, has been found in N-A-S-H gel [58,61,63], but was not found in [57,60]. Despite maintaining a 3D structure, a lower Si/Al ratio in N-A-S-H gel can result in a more compact structure with more Q^3 and Q^4 [57,58]. Water content also affects the structure of N-A-S-H gel. Lyngdoh et al. [74] claimed that a high water content decreases Q^4 and Al(V), while the results by Zhang et al. [63] were partly contradictory, showing more Al

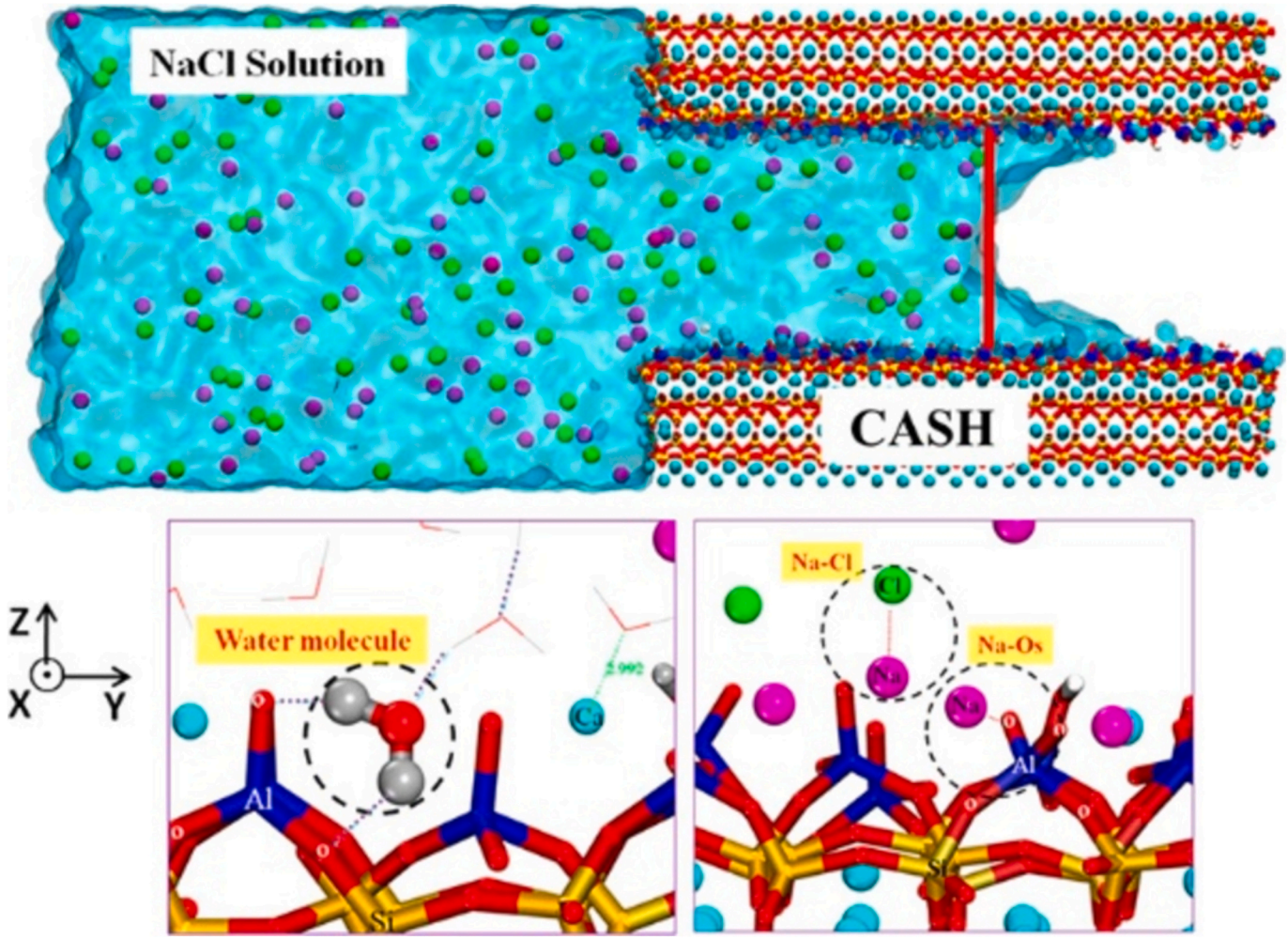

Fig. 4. Schematic representation of the transport of NaCl solution within C-A-S-H gel pores [43].

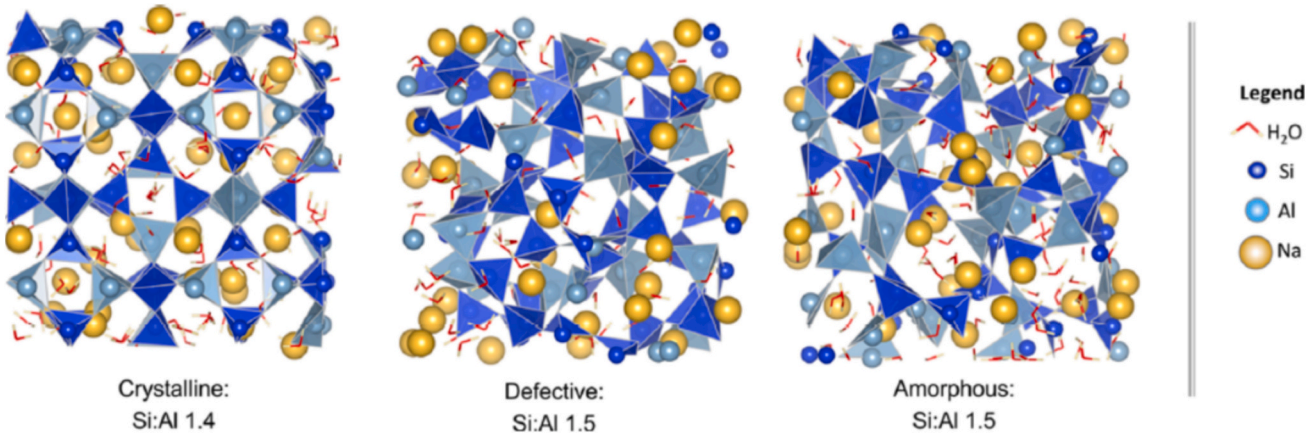

Fig. 5. Model structures of N-A-S-H with different degrees of disorder [60].

(V) in the structure of N-A-S-H gel compared with that in the sodium aluminosilicate (N-A-S) without water. Apart from that, the positioning of water was found to affect the medium-range structure of N-A-S-H gel [75]. The structure factor of N-A-S-H gel with interlayer water matched well with neutron pair distribution function (PDF) experimental results. The soundness of N-A-S-H gel models can also be validated by comparison with various other experimental results including XRD [58,62], FTIR [76], and NMR (Q^n fractions) [57,58]. Although some inconsistent results have been found, probably due to different construction methods and force fields, the overall understanding of the structure of N-A-S-H gel has been improved through atomic simulation. It is, however, essential that in the construction of N-A-S-H model, the role and importance of water can be described correctly through careful model design; some published studies which present an anhydrous amorphous N-A-S phase and claim that it represents AAM binding phases are likely to introduce structural errors for this reason, and must be viewed with

caution.

The mechanical behaviors of the N-A-S-H gel, including properties such as elastic modulus, tensile strength and fracture toughness, have been mainly studied by a tensile deformation test in MD simulation. It has been found that the mechanical properties of N-A-S-H gel are significantly affected by its chemical composition. There is still a debate about the optimal Si/Al ratio to obtain maximum elastic modulus and tensile strength [61,62,65]. The tensile strength of N-A-S-H gel is believed to be influenced by the fractions of penta-coordinate Al, bridging oxygens, and Si-O-Si bonds [61,65], while the elastic modulus is more related to the fraction of hydroxyl groups and network complexity [65]. Increasing water content in N-A-S-H gel also resulted in a decrease in its tensile strength [63,64]. Fracture toughness of N-A-S-H gel has also been calculated from the simulated tensile stress–strain curves (see Fig. 6) in [74], and showed a good correlation with the available experimental results [67]. Sadat et al. [76] carried out a simulated nano-indentation test via MD to study the mechanical properties of the N-A-S-H gel, and found that the hardness of N-A-S-H gel is strongly dependent on the indenter size, loading rate, and Si/Al ratio. The interfacial interactions between N-A-S-H gel and fibers have also been studied through a simulated pull-out test using MD [77]; again, the Si/Al ratio and internal moisture content in N-A-S-H gel significantly influence the bonding strength between N-A-S-H gel and the fiber.

Atomistic simulation of N-A-S-H gel can also provide valuable insights into the mechanisms that control durability-related performance aspects of geopolymers. The adsorption and mobility of ions are critical concerns because they are closely related to leaching, immobilization, and chemical attack. The mobility of sodium was reported to decrease with an increase in the Si/Al ratio, because the N-A-S-H gel tends to form a structure with more small rings, thereby limiting the mobility of sodium [68]. It was also found that increasing water content promoted the diffusion of sodium [64,68]. However, the opposite trend was reported in [63], which claimed that sodium in N-A-S-H became much more stabilized in the presence of water due to the formation of Na-OH bonds and enhancement of the electrostatic attraction between sodium and AlO_n units. Resolving these discrepancies between different studies could help to explain the alkali leaching and/or efflorescence problems faced by some geopolymers in service, but needs further development.

As shown in Fig. 7, leaching behavior of Na from the N-A-S-H matrix to a bulk solution has been simulated in [69], which modeled the attack of Na_2SO_4 and $MgSO_4$ solutions on N-A-S-H gel. Chloride ions are weakly adsorbed by N-A-S-H gel, as the intrinsically negatively charged aluminosilicate surface does not attract the chloride ion [70], and the single positive charge on the sodium ions does not provide a high degree of charge screening or reversal in a double layer as is the case for higher-charged cations such as calcium. Bagheri et al. [71] also confirmed that chloride ion has less interaction with N-A-S-H gels at lower chloride concentrations or at higher temperatures.

The thermal resistance of N-A-S-H gel is also a topic of interest. Hou et al. [72] found that the structure of N-A-S-H gel at high temperatures became less connected, resulting in a reduction of its tensile strength and stiffness. However, the high temperature was found to contribute to a higher toughness of N-A-S-H gel.

Overall, atomistic simulations of N-A-S-H gel can offer some meaningful perspectives into the design of geopolymer materials with desired engineering properties, although with the obvious limitation that they cannot capture microstructural (or larger-length scale) influences on engineering properties. Some inconsistent results in the literature are mainly attributable to variations in the employed force fields, in simulation setup decisions by different researchers, and other factors. Generally, the accuracy of the simulation enhances successively when utilizing the DFT method, followed by ReaxFF, and then traditional force fields. Nonetheless, it is crucial to acknowledge that the choice of simulation method entails trade-offs. While high-accuracy methods like DFT can improve precision, they come at the cost of restricted model size and reduced computational efficiency. Striking a balance between accuracy and computational resources is essential. To further enhance the credibility of these simulations, further work should focus on comparing and validating the results with additional experimental data. The gap between the nano-scale and larger scales needs to be further explored in order to gain a deeper understanding of the behavior of N-A-S-H gel, and its implications for practical applications.

3. Thermodynamic modeling of AAMs

Thermodynamics plays an important role in understanding and describing the chemical reactions occurring in construction materials [78]. As illustrated in Fig. 8, the chemical reactions involved in AAMs also follow the laws of thermodynamics, although kinetic factors are clearly important. The relatively close approach to (stable or metastable) equilibrium that is observed through many stages of the reaction processes makes this a valuable tool in the analysis of AAMs.

Aluminosilicate precursors in AAMs start to dissolve as soon as they are mixed with an alkaline activator solution, because the aqueous phase is highly undersaturated with respect to the solid phases present, elevating the concentrations of aqueous ions in solution (see the red dashed curve). This process corresponds to the dissolution kinetics, continuously releasing the constituents of precursors into solution.

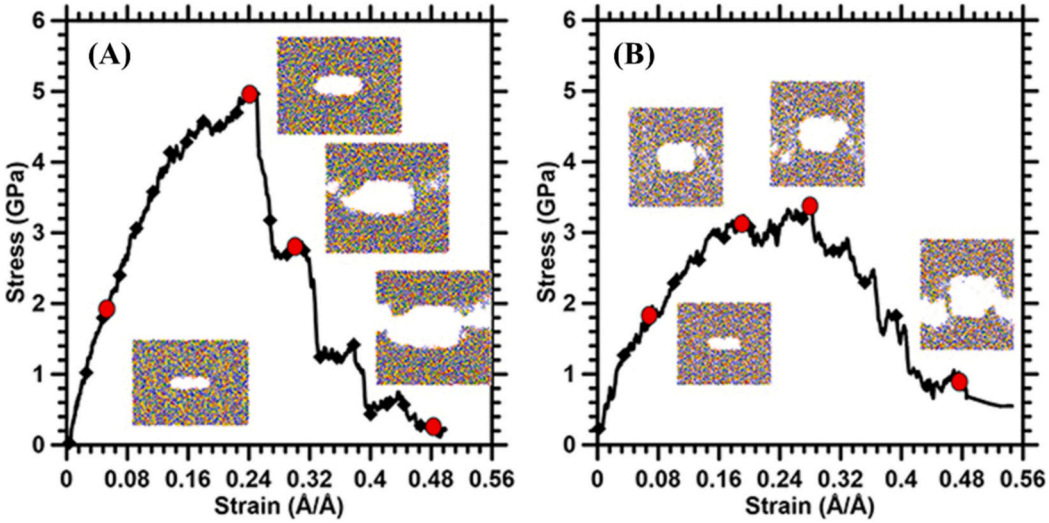

Fig. 6. Tensile stress–strain response of the N-A-S-H structure with an initial flaw, for (A) 15% water content and (B) 20% water content [74].

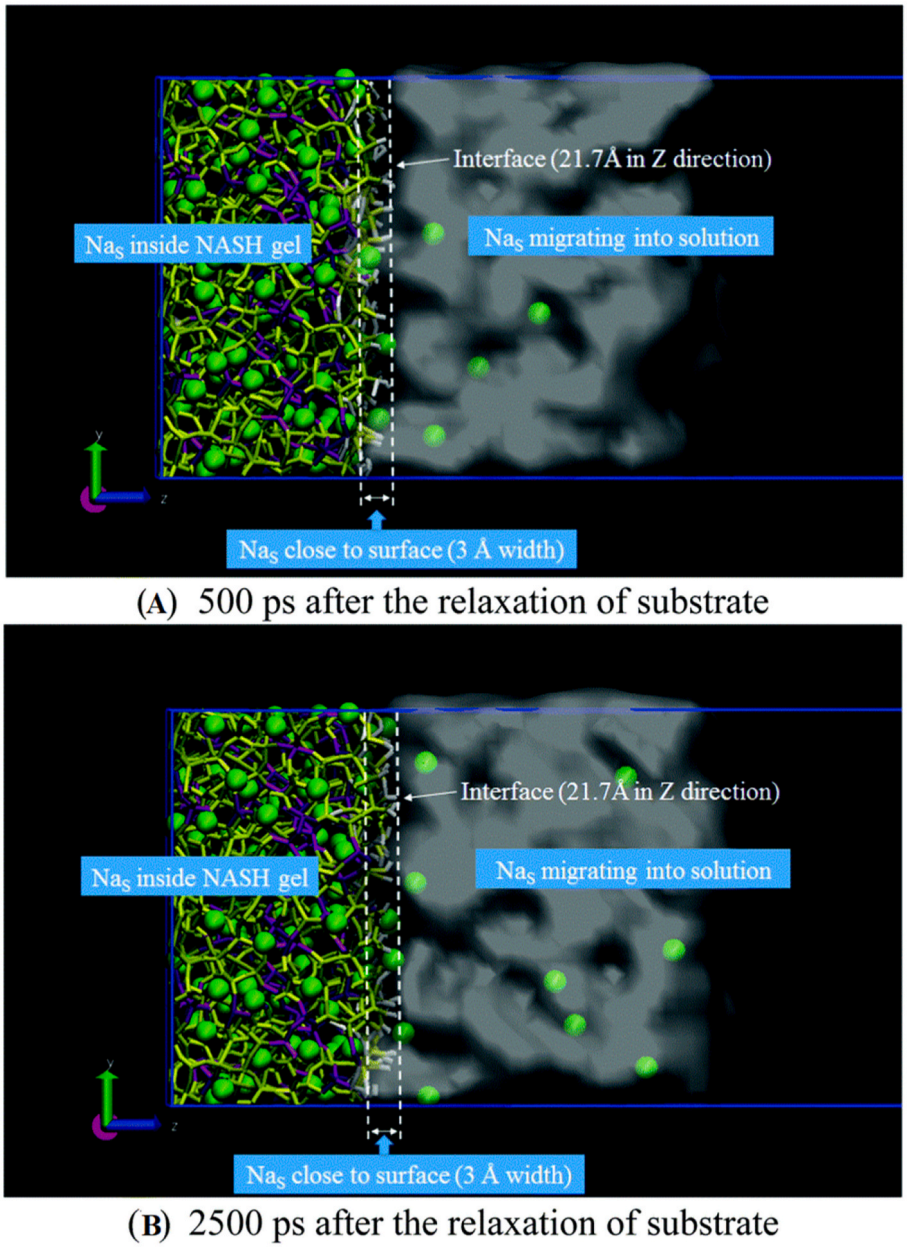

Fig. 7. Snapshots of Na in the NASH matrix migrating into solution [69].

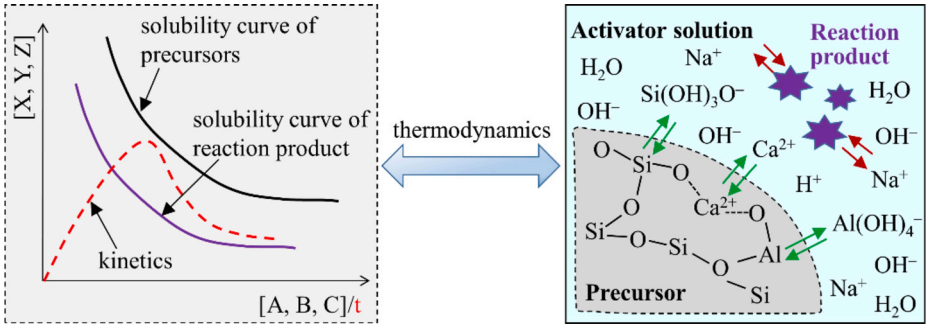

Fig. 8. A schematic representation of the application of thermodynamics in analyzing the reactions of AAMs. In the graph, [X, Y, Z] and [A, B, C] indicate the concentrations of aqueous ions X, Y, Z and A, B, C, respectively, and t is time that corresponds to the red dashed curve (*kinetics*).

When the solution becomes saturated or supersaturated, specified solid reaction products thermodynamically tend to precipitate, with the consumption of aqueous ions that reduces the degree of supersaturation. According to the Ostwald step rule [79], the initially-formed solid phases are likely to be less stable than the final thermodynamically preferred products, and so it is possible that these will either evolve or re-form toward more stable structures. As a result, the concentrations of these aqueous ions in solution turn to decrease. Overall, the system will progressively evolve toward a state that minimizes its Gibbs free energy, although this process is subject to kinetic constraints that may, for example, greatly slow down dissolution reactions at later age due to surface blockage by dense reaction products. The precursors, which are intrinsically less stable (more reactive), are transformed to more stable binding phases.

Thermodynamic modeling of AAMs is usually performed using software tools by specifying a certain reaction degree of the precursors (i.e. describing kinetic effects essentially as an input to the thermodynamic model, potentially by passing information from a separately-calculated kinetic model). At each specified extent of reaction, equilibrium between the solution and the solid reaction products is assumed. The accuracy and reliability of thermodynamic modeling results are determined by whether this assumption is sufficiently accurate under the given circumstances – and this is controlled in many simulations of cementitious materials by manually preventing the formation of certain phases which are known to form only very slowly – as well as the quality and completeness of the thermodynamic database for all constituents of the system, and the appropriateness of the activity coefficient model that is applied to describe non-idealities in the aqueous phase in particulate.

3.1. *Thermodynamic database for AAMs*

The thermodynamic database used to model AAMs is usually established based on the databases for PC-based materials, supplemented by introducing the solid phases that are uniquely identified as reaction products in AAMs depending on their calcium content [16,80,81]. As shown in Fig. 9, any of these unique phases can be included in the thermodynamic database, once their thermodynamic data are defined.

In experimental characterization of alkali-activated high-Ca systems (most commonly alkali-activated slag), C-(N-)A-S-H gel and Mg-Al layered double hydroxide (LDH) phases are identified as the key reaction products. In thermodynamic modeling of high-Ca AAMs, Myers et al. proposed ideal solid solution models CNASH_ss and MgAl-OH-LDH_ss to describe C-(N-)A-S-H gel and Mg-Al LDH phases, respectively [82,83]. The CNASH_ss model consists of eight end-members while the MgAl-OH-LDH_ss model contains three end-members. The thermodynamic properties (data) of those end-members were provided in [82,83]. The CASH+ model [84], designed for blended Portland cements, has also been extended to describe alkali substitution to form C-(N-)A-S-H; other alkali and alkali-earth cations are also allowed in that model to substitute into the interlayer of C-A-S-H using a sublattice-based structural description. The thermodynamic database Cemdata18 [85] includes these reaction products, enabling its use in modeling Ca-rich-alkali-activated materials. It is maybe important to note at this point that thermodynamic modeling of alkali-activation of blast furnace slag often leads to the prediction that a large quantity of strätlingite will form at equilibrium. This trend is not generally reflected in experimental results, and this requires further investigation on both experimental and theoretical (database refinement) aspects, to resolve any uncertainty that exists.

N-A-S-H gels can form in parallel with these products in some activated slag or blended AAM binders [24], and as noted above, these can either be described by analogy to zeolites, or modeled directly by using the growing body of solubility data available for them [86–88]. The thermodynamic properties of zeolites and similar phases, for example hydroxysodalite, Na-chabazite and zeolite P, and their potassium-containing counterparts, have been determined [89], and are incorporated into the zeolite20/zeolite21 database which is consistent with Cemdata18 [90,91]. Other reaction products, such as calcium carbo−/sulfo-aluminate hydrates, hydrogarnets, and strätlingite, already exist in the thermodynamic database that is used for thermodynamic modeling of PC-based materials.

In alkali-activated low-Ca system with low to no calcium content in the precursors (e.g. alkali-activated fly ash or metakaolin), N-A-S-H gel is the primary, and often unique, reaction product. The other possible reaction products are mostly zeolites. However, the thermodynamic properties of N-A-S-H gel are less well known than C-(N-)A-S-H gel. The reason for this is the structurally disorder in the highly cross-linked aluminosilicate N-A-S-H gel, whose chemical composition depends on the precursor composition and alkali activation conditions [17,18]. Based on literature studies regarding the structure [92,93] and chemical composition [18,94,95] of N-A-S-H gel, Zuo proposed a solid solution model N(*C*)ASH_ss to describe the N-A-S-H gel in thermodynamic modeling of low-Ca AAMs [96]. This model contains eight end-members and their thermodynamic properties can be found in [96]. Among these solid solution end-members, the first four end-members are used to describe the N-A-S-H gel, while the other four end-members are used to consider the partial uptake of calcium by N-A-S-H gel due to the interactions between the N-A-S-H gel and the aqueous calcium. In the N(*C*)ASH_ss model, a 90% replacement of Na by Ca was applied according to [97]. However, this replacement ratio is in doubt and the amount of Na in the N-A-S-H that could be substituted by Ca needs further research. In a recent study, Chen et al. synthesized N-A-S-H with various Si/Al ratios and established their thermodynamic data, which contributes to a step further in the advancement of thermodynamic modeling of low-Ca

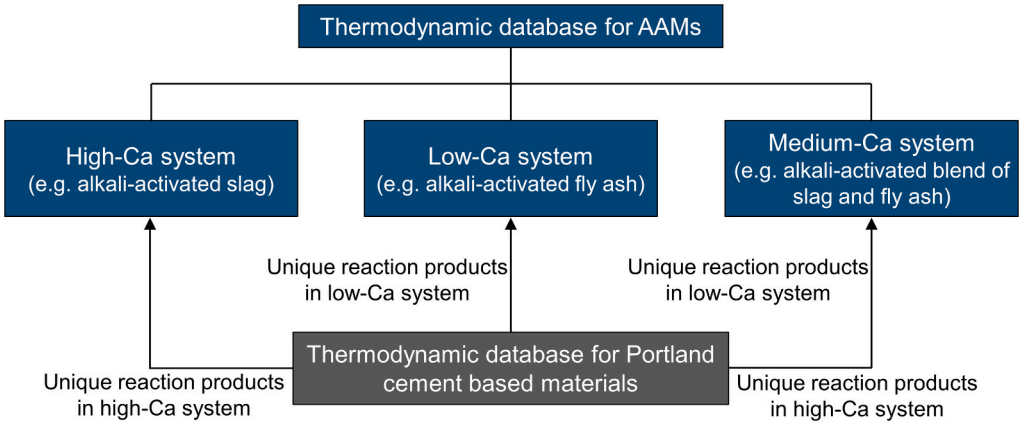

Fig. 9. Construction procedure of the thermodynamic database for AAMs.

AAMs [86].

In addition to low- and high-Ca type AAMs, high-Fe AAMs are gaining increasing attention in the scientific literature [98]. In comparison to other main cementitious elements, such as Ca, Si and Al, the modeling of Fe uptake is more challenging because the reduction-oxidation potential of the system affects the aqueous speciation of Fe and the precipitation of Fe-containing phases. The Fe-containing phases mainly include Fe-Al-hydrogarnets [85], C-F-A-S-H gel [99], N-(A, F)-S-H gel [100], and N-F-S-H gel [101]. While Fe-containing hydrates, such as Fe-Al-hydrogarnets, are included in the Cemdata18 database for PC-based materials, appropriate thermodynamic data for high-Fe AAMs are either missing or (in some cases) identified as needing reassessment [102]. This is an important avenue for future advances in database development.

3.2. Approach of thermodynamic modeling

Thermodynamic calculations of cement solubility and precipitation processes are commonly conducted using two distinct, but complementary approaches. In software tools such as GEM-Selektor V3 (http://gems.web.psi.ch/) [103,104], a system of equations describing the Gibbs free energy of the reaction system is established, and then the Gibbs energy is minimized by manipulating the species and phases present (while maintaining correct mass balance as a constraint); the combination of dissolved species and solids that gives the lowest Gibbs energy is defined as being the equilibrium state. Conversely, software tools can also use the law of mass action (i.e. linking aqueous and solid compositions via defined equilibrium constants for a set of possible reactions) to search for an equilibrium state; PHREEQC [105] is a popular implementation of this approach. Both approaches should in principle give similarly correct outcomes if a high quality database (such as Cemdata18, which is available in both GEM-Selektor and PHREEQC formats) is selected, and if a sufficiently rigorous activity coefficient model is used to describe the aqueous phase. It is noted that the thermodynamic properties of phases in the thermodynamic database are usually determined at 25 °C. The thermodynamic data for solids other than 25 °C are derived from the data at the reference temperature (25 °C) by a series of formulas. More details of the derivation can be found in [106,107].

In simulating cements, various relationships based on extensions of the Debye-Huckel equation are often used to calculate the ion activity coefficients. Eq. (1) gives one such model, the Truesdell-Jones formulation, which is often used in GEM-Selektor models for Portland cement hydration [108]:

$$Log_{10}\gamma_j = \frac{-A_\gamma z_j^2\sqrt{I}}{1+\dot{a}B_\gamma\sqrt{I}} + b_\gamma I + log_{10}\frac{x_{jw}}{X_w} \quad (1)$$

where γ_j and z_j are the activity coefficient and charge of the aqueous species j, respectively. A_γ and B_γ are electrostatic parameters, I is the ionic strength of the aqueous electrolyte phase, x_{jw} is the mole quantity of water and X_w is the total mole amount of the aqueous phase. $\dot{a}$ and b_γ are the average ion size and the parameter for common short-range interactions of the charged species.

Eq. (1) is generally considered to be useful up to ionic strengths of around 1 mol/kg H_2O [108]; this is sufficient to describe Portland cement hydration, but in the early stages of reaction of AAMs, the ionic strength may be significantly higher, often up to 3 mol/kg H_2O [21,109]. Activity coefficients in more concentrated solutions can be determined by using the Pitzer model [110], which is intended to be applicable up to ~6 mol/kg H_2O [111], but which is rather complex in its parameterization and implementation. In the context of cements including AAMs, most thermodynamic modeling studies usually assume that using Eq. (1) to calculate ion activity coefficients would not significantly affect the modeling results. However, a recent thermodynamic modeling study reported an absolute difference of 2.5 g in the reaction products at early age for the activation of 100 g of slag, when comparing thermodynamic calculations using the Pitzer model and Eq. (1) [112]. To improve the accuracy of thermodynamic modeling results, it is recommended to more widely implement the Pitzer model, particularly for modeling AAMs at early age with high ionic strength pore solutions.

3.3. Application of thermodynamic modeling to AAMs

Thermodynamic modeling has been applied for over 15 years [109] to the analysis of several types of AAM formulation, particularly at the higher-calcium end of the compositional range, where the C-(N-)A-S-H models described above can be applied to describe the main reaction product. Myers et al. [24,82,83] predicted the phase diagrams of alkali-activated slag cements under various alkali activation conditions and with different chemical compositions of slag. Taking a sodium silicate activated slag as an example, Fig. 10 presents its phase assemblage evolution as a function of the degree of slag reaction by using thermodynamic modeling [83]. The predicted phase assemblages agreed relatively well with those determined experimentally [35,113,114]. Following these works, many other researchers have also performed thermodynamic modeling of alkali-activated slag cement, focusing on phase evolution and related physicochemical properties. Ye and Radlińska [115] used thermodynamic modeling to investigate the chemical shrinkage of alkali-activated slag and reported a prediction error margin of 5–19%. By combining a thermodynamic approach with a governing equation for reaction kinetics (see [29] for more discussion of this topic), Zuo et al. [116] performed thermodynamic modeling of alkali-activated slag over a time scale representing the reaction process, evaluating the pore solution chemistry, chemically bound water of C-(N-)A-S-H gel, reaction products assemblage, and chemical composition of the reaction products. This body of work has suggested that thermodynamic modeling is able to predict and investigate the physicochemical properties of alkali-activated slag cement.

Thermodynamic modeling has also been used to investigate the interactions between alkali-activated slag cement and potentially aggressive agents, to predict the durability of AAMs exposed to single or multiple factors [117–121]. Among those studies, Ke et al. [117] proposed a thermodynamic model to describe carbonate intercalated hydrotalcite and used this information to describe the phase assemblage change in alkali-activated slag cements when exposed to CO_2 (see Fig. 11). The modeling results show that the slag chemistry significantly impacts the mass fractions of carbonation products that form, while the nature of the alkaline activator influences the phase evolution process and changes in pore solution pH under carbonation. For instance, the pore solution of sodium carbonate activated slag exhibited a higher pH than that of sodium silicate activated slag at the same carbonation degree. Later, Zuo established thermodynamic models to describe chloride- and sulfate-intercalated hydrotalcites, and investigated the phase diagrams of alkali-activated slag cements subject to attack by chloride salt [118], sulfate salt [119], and both of these together [121]. The prediction results agree well with the experimental data retrieved from the literature, and it is interesting to note that the combined attack of chloride and sulfate salts exhibited additional coupling effects which promoted the formation of chloride-containing hydrotalcite and inhibited the formation of Friedel's salt and magnesium silicate hydrate. Additionally, Mundra et al. [122] used thermodynamic modeling to establish a lookup table-style database of binder mineralogy and pore fluid compositions for use in simulating the transport properties and mineralogical evolution of AAMs under chloride attack.

Conversely, the thermodynamic modeling of low-Ca and medium-Ca AAMs is rarely reported in the literature. This is mainly due to the lower availability of thermodynamic data for low-Ca AAMs, although efforts to resolve this deficit are underway in multiple laboratories worldwide. Based on the experimentally determined solubility products of synthesized N-(C-)A-S-H [86], Chen et al. conducted thermodynamic modeling

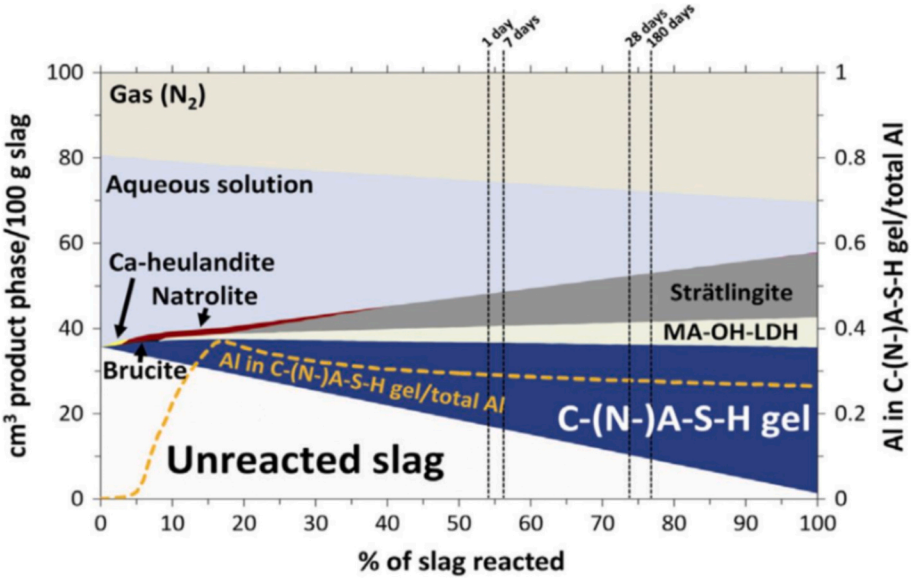

Fig. 10. Thermodynamic modeling of a sodium silicate activated slag predicts the phase assemblage (in the calculations, water/solid = 0.4, Na_2O/slag = 4%, Na_2O/SiO_2 = 1) [83].

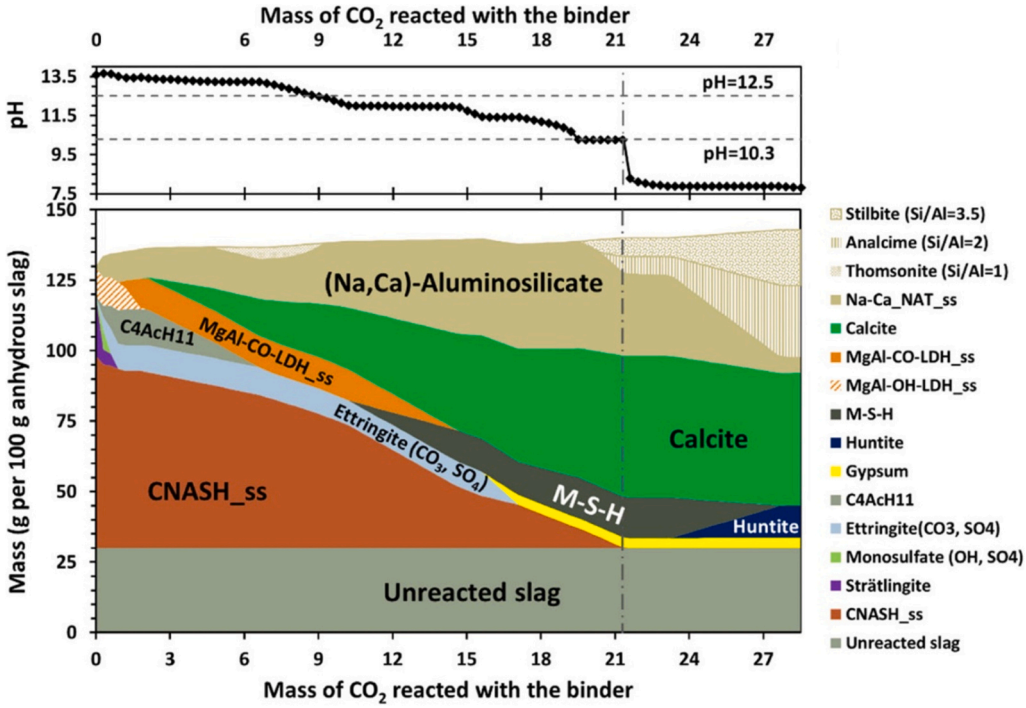

Fig. 11. Thermodynamic modeling of the phase evolution and pore solution pH value of sodium silicate activated slag cement under stepwise accelerated carbonation (in the calculations, water/solid = 0.40, Na_2O/slag = 4%, Na_2O/SiO_2 = 1, reaction degree of slag = 70%, and concentration of CO_2 = 1%) [117].

of alkali-activated fly ash and reported that the modeled compositions of the solid reactions products and pore solution are well aligned with the experimental ones [123]. Zuo conducted thermodynamic modeling of low-Ca and medium-Ca AAMs as shown in Fig. 12 [96]. For the alkali-activated fly ash, the modeling results showed that an increase in the content of Na_2O in the alkali activator decreased the formation of N-(C-)A-S-H gel, while an increase of the alkali activator modulus resulted in its increased formation. These modeling results are consistent with experimental observations [124]. For the alkali-activated slag-fly ash blend, the modeling results showed the co-existence of C-(N-)A-S-H and N-A-S-H gels, with C-(N-)A-S-H making a greater volumetric contribution to the system than N-A-S-H, aligning with the experimental findings [16,80,81]. Recently, Chen et al. [125] used the N(*C*)ASH_ss model to simulate the phase assemblages of alkali-activated municipal solid waste incineration (MSWI) bottom ash pastes, and concluded that the modeling results can be used as references for the mix design of MSWI bottom ash based AAMs. It is worth noting that the N(*C*)ASH_ss model for describing the N-A-S-H gel was established semi-empirically based on experimental observations, and its accuracy thus depends on the quantity and quality of experimental data that were used to derive the model. Although the modeling results show a satisfactory agreement with experimental observations, more experimental solubility data are

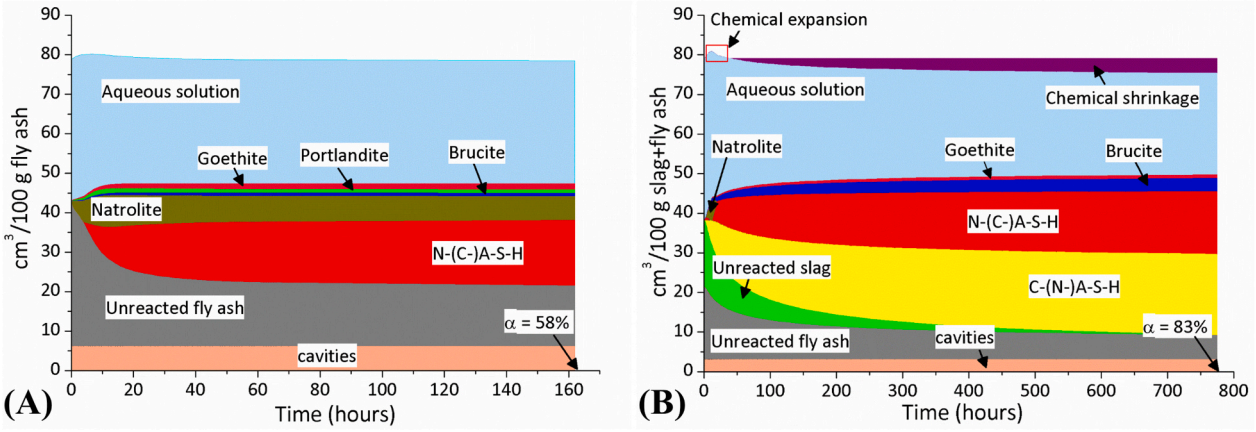

Fig. 12. Simulated phase evolution of (A) sodium hydroxide activated fly ash and (B) sodium silicate activated slag-fly ash blend (in the calculations: (A) water/fly ash ratio═0.35, Na_2O/fly ash ratio═6.2%, and reaction temperature = 60 °C; (B) slag/fly ash = 1:1, water/binder ratio = 0.40, Na_2O/binder ratio = 6%, activator modulus = 0.93, and reaction temperature = 20 °C) [96].

needed for improving the thermodynamic data quality of N(*C*)ASH_ss in support of modeling of lower-calcium AAM binders.

So far, thermodynamic modeling has been widely used to investigate high-Ca AAMs and achieved fruitful results, while it is still limited for low-Ca and medium-Ca AAMs due to the underdeveloped thermodynamic model for describing the N-A-S-H gel. Thus, more work should be devoted to the development of a thermodynamic model for the N-A-S-H gel and thermodynamic modeling of low-calcium AAMs. The phase evolution of AAMs involves the coupling of thermodynamics and kinetics, particularly for the cases of interactions with aggressive environmental conditions. However, the current thermodynamic modeling of AAMs does not in general feature detailed kinetic descriptions, which introduces some uncertainty into the models. Therefore, kinetic issues, such as the dissolution rate of aluminosilicate precursors, reaction rate, and diffusion coefficients, should be taken into account in future thermodynamic studies where possible. In studying the durability performance of AAMs, the phase evolution, microstructural damage, and ionic transport are inter-dependent aspects, and more efforts should be devoted to interconnecting their respective effects in establishing a chemical-damage-transport model. Last but not the least, thermodynamic modeling shows great potential in guiding mix design of AAMs [126], and thus more work are recommended in this regards.

4. Simulation of the microstructure formation and microstructure-based modeling of AAMs

With the continuous growth of reaction products as precursors dissolve and binding phases precipitate, the microstructure of AAMs forms. During this process, capillary and gel pores are gradually filled and blocked, resulting in a finer and finer pore structure. The microstructure as well as the pore structure of AAMs have substantial effects on the mechanical properties (e.g. strength and fracture energy etc.) [127], volume stability (e.g. shrinkage and creep properties) [128], and durability performance (e.g. resistance to transport of water and ions) [129]. Therefore, microstructure-related numerical research on AAMs has attracted increasing attention. The current numerical studies of the microstructure of AAMs can be mainly grouped into: (i) simulation of microstructure formation, and (ii) microstructure-based modeling of material properties.

4.1. Simulation of the microstructure formation of AAMs

Many numerical models to simulate the micro- and pore structure development of PC-based materials have been developed and published. For instances, CEMHYD3D [11], μic model [130] and HYMOSTRUC [10] are three of the most widely used numerical modeling frameworks for studying the microstructure formation of PC-based materials. However, these were originally designed for PC-based materials and are therefore not directly capable of numerically studying the microstructural evolution of AAMs. This is because the raw materials, reaction mechanism and microstructural development of AAMs are inherently different from those of PC-based materials, as discussed above. In this situation, it is necessary to develop the model from a new modeling point of view by considering the intrinsic characteristics of AAMs. To date, however, few models have been reported that describe the simulation of the microstructural formation of AAMs; the GeoMicro3D model is one such model that is available [96]. In the following paragraphs, this review will introduce and discuss the GeoMicro3D model and its potential limitations that require further research efforts.

The microstructural development of AAMs is accompanied by a number of physical and chemical processes. These include the initial geometrical particle arrangement of precursor grains within the alkaline activator solution, dissolution of precursor grains, diffusion/transport of aqueous ions, chemical reactions of ions, and nucleation and growth of reaction products. These processes are interdependent and determine the microstructural evolution of AAMs. By modeling these processes, Zuo and Ye [131] proposed a novel framework (GeoMicro3D) for developing numerical models to mimic the microstructure evolution of AAMs. Fig. 13 illustrates the scheme of this numerical framework, which consists mainly of five numerical modules. The first module aims to generate the initial structure of real-shaped precursor grains within a volume of alkaline activator solution. The second module simulates the dissolution process of precursor grains. The third module simulates the transport of aqueous ions using the lattice Boltzmann method. In the fourth module, the reactions of aqueous ions are simulated and the corresponding reaction products are quantified by means of thermodynamic modeling. In the last module, a nucleation probability theory is applied to account for the nucleation and growth of reaction products in the simulation system. In this way, the reaction process and the microstructural evolution of AAMs can be numerically simulated.

Later, Zuo et al. [96,132] implemented this numerical framework to simulate the reaction process and microstructure evolution of alkali-activated slag. The simulation results were discussed and compared with the relevant experimental data, such as the degree of reaction of slag and the composition of the pore solution, demonstrating a good agreement between the comparisons. Fig. 14 shows an example of the simulated microstructures and their corresponding pore size distributions for an alkali-activated slag cement paste at different curing times. These images show that reaction products grow, the microstructure evolves, and thus the pore structure gradually refines over time. In

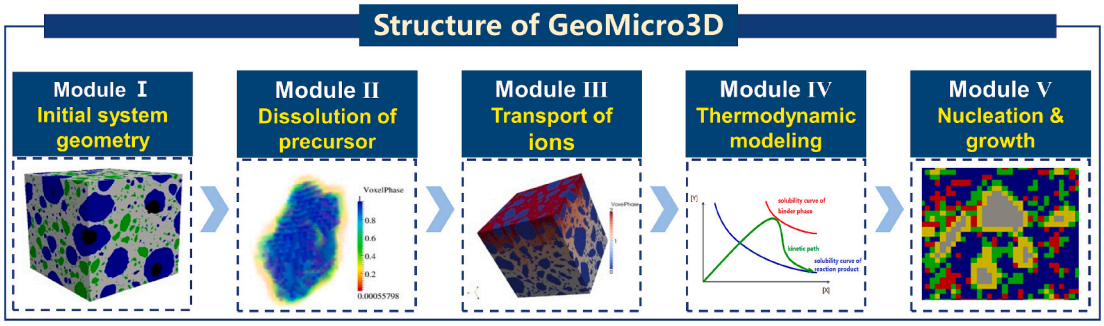

Fig. 13. Modeling scheme of the microstructure in AAMs [131].

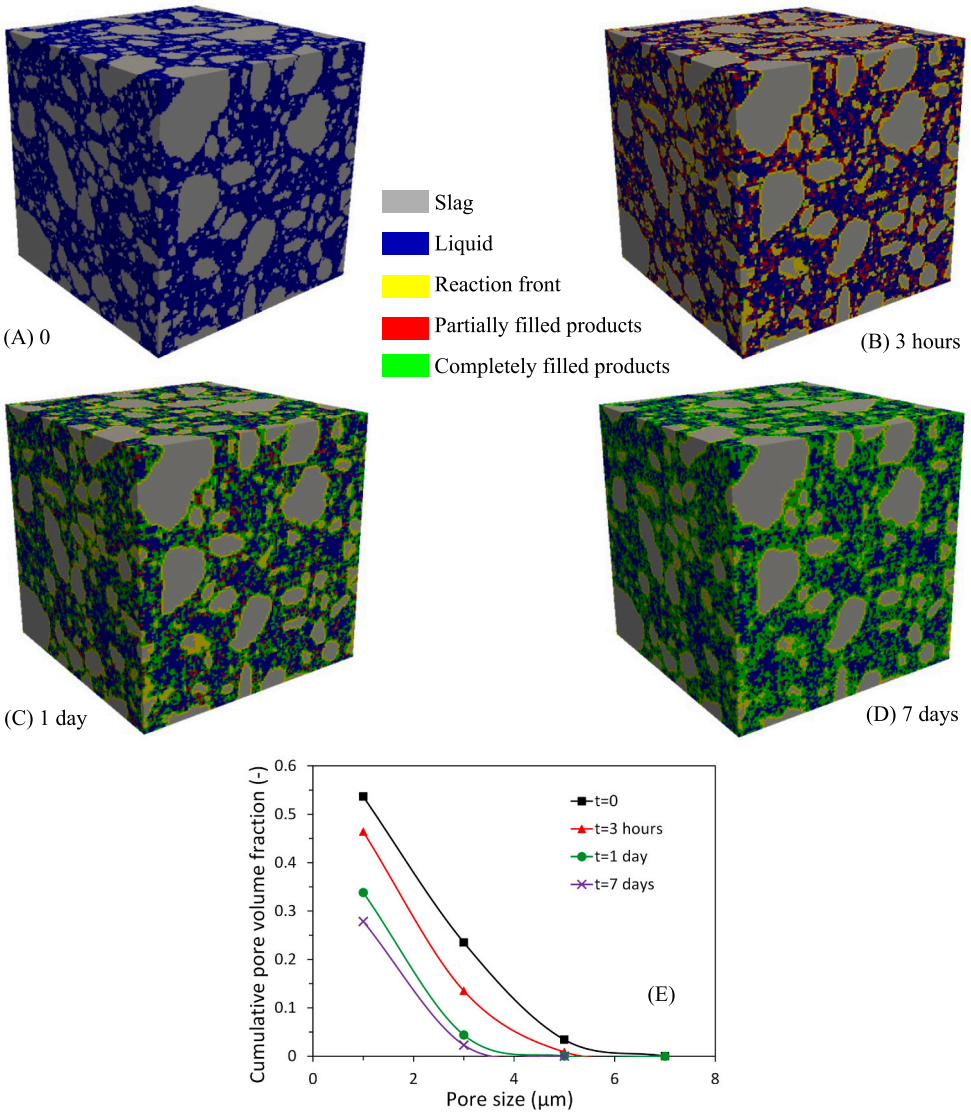

Fig. 14. Simulated 3D microstructures and particle size distributions of an alkali-activated slag paste at different curing times, using the GeoMicro3D model [96,132].

addition to the microstructural evolution, more information about reaction kinetics, pore solution chemistry, and volume evolution of phases can also be simulated, and water permeability and chloride diffusivity can also be described. A detailed comparison and discussion of these aspects can be found in [96,132]. In a recent study, GeoMicro3D was implemented to study the reaction and microstructure development of one-part alkali-activated slag and the results demonstrated the rationality of this model [133].

Although the GeoMicro3D model has been successfully implemented to study the alkali-activated slag system, it still needs to be improved and extended further. In addition to those already mentioned, the following are three important aspects to which more efforts should be directed in the future:

- *Heterogeneous phase distribution of phases in precursors*: When GeoMicro3D was implemented for the simulation of alkali-activated slag, the distribution of elements in the slag was assumed to be homogeneous. This modeling strategy sounds reasonable as slag consists of >95% vitreous phase. However, it should be noted that fly ash grains typically contain about 30% of crystalline phases in addition to the vitreous phase (or phases) present. Furthermore, the vitreous and crystalline phases in fly ash are heterogeneously distributed (see Fig. 15). Obviously, the heterogeneous distribution of phases affects the dissolution kinetics of fly ash, which further has a significant impact on the geopolymerization process and microstructure development of alkali-activated fly ash [134]. Therefore, future work should be undertaken to consider the heterogeneous distribution of phases in precursors when modeling the dissolution process of precursors in the implementation of GeoMicro3D.

- *Relaxation time scheme*: Computational efficiency is an important aspect that a numerical model should consider. In GeoMicro3D, AAMs are digitized into lattice cells and the lattice Boltzmann method is used to simulate the transport of ions. A single relaxation time scheme was used to simplify the implementation of this method. However, according to [136], this implementation is not computationally efficient as it requires a large number of iterations. Conversely, multi-relaxation time schemes could reduce the number of iterations needed to reach the steady state [136]. Therefore, the application of multi-relaxation time schemes should be considered as a way to improve the computational efficiency.
- *Model parameters*: The GeoMicro3D model has many model parameters. However, most of these parameters were unknown. To address this issue, a parametric study was carried out by comparing the simulation results with experimental data. In future work, alternative techniques should be preferred to be used to determine these parameters, such as the determination of nucleation parameters by experiments [137], and more importantly a detailed parameter sensitivity analysis should be performed to improve the reliability of GeoMicro3D.

4.2. Microstructure-based modeling of AAMs

AAMs, like PC-based materials, are porous materials and therefore their microstructure dictates the development of their mechanical and durability properties. Many microstructure-based modeling studies have been reported for PC-based materials in terms of tensile strength [138,139], permeability [140,141] and diffusivity of chloride [142,143] etc. However, few microstructure-based modeling studies have been carried out for AAMs. In an early study, Provis et al. [144] used synchrotron X-ray computed tomography (XCT) to determine the microstructure and pore network geometries of various alkali-activated binders as a function of age and slag/fly ash ratio, and used random walker simulations within those reconstructed pore networks to define parameters related to pore tortuosity. Das et al. [145] also used synchrotron XCT to reconstruct the 3D microstructure of alkali-activated fly ash paste, based on which the intrinsic permeability was numerically predicted to be 5×10^{-14} m^2 by using a numerical Stokes solver [146]. The detailed procedure used by those authors is shown in Fig. 16.

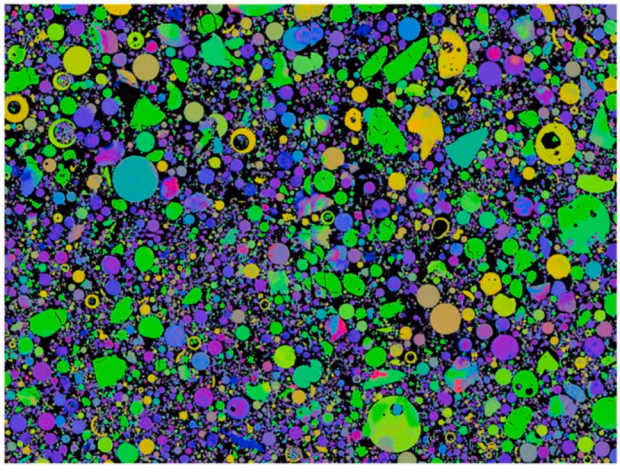

Fig. 15. Heterogeneous distribution of elements in fly ash as visually indicated by different colors [135].

Based on the GeoMicro3D platform, a numerical model to investigate the chloride transport in AAMs was proposed and implemented to simulate chloride transport in alkali-activated slag cement paste [147]. The effective diffusivity in the paste was simulated to be between 6×10^{-13} and 5×10^{-12} m^2/s, which is reasonable as compared to the values reported in concrete (10^{-12} to 10^{-11} m^2/s) [148,149]. These studies, although still limited in number, demonstrate that the microstructure-based modeling has promising potential for investigating the transport properties of AAMs.

Although the 3D microstructure of AAMs can potentially be determined by using XCT, it is quite challenging to identify and classify phases in XCT images. This is because the absorption contrast in the available X-ray energy range tend to be low (particularly for low-calcium AAMs which are dominated by the light elements Si, Al, Na, and O), and the microstructure of AAMs is complex, making it difficult to classify and identify phases [145], although novel approaches based on artificial intelligence are now being applied to give advances in this area [150].

5. Multiscale modeling of AAMs

The different chemical compositions of the two types of gels formed in AAMs inherently lead to differences in their structures and properties. Therefore, reliable modeling strategies for AAMs should link the binder chemistry and the resulting nano- or microstructural features with engineering properties at the macroscopic scale. An accepted modeling strategy is multiscale modeling, which aims to link multiple scales of observation of a material. Multiscale modeling can be achieved using a variety of approaches, including hierarchical modeling and concurrent multiscale modeling [151–153]. Such models have been widely applied to estimate the mechanical properties and volume stability of PC-based materials, such as elastic modulus [154–156], strength [157,158], autogenous shrinkage [159], and creep properties [160,161]. In the current literature as reviewed so far, multiscale modeling of AAMs mostly focuses on the mechanical properties by using analytical micromechanics and homogenization theory.

Šmilauer et al. [162] applied semi-analytical homogenization to alkali-activated fly ash and metakaolin. A two-scale micromechanical representation of the materials was proposed, distinguishing between N-A-S-H level and the paste level. The N-A-S-H level consists of poorly crystallized reaction products, introduced as solid gel particles, while the paste level includes unreacted material grains as well as the open porosity. The time-evolving phase volume fraction of the solid gel particles captured the stiffening of the N-A-S-H gel. The modeling results were compared with the experimental data, showing a good agreement in general. The proposed model is sufficiently versatile to include different low-Ca-type AAMs with a range of activator compositions, and different mixing proportions. However, recalibration and kinetic monitoring are still necessary prior to modeling.

Das et al. [145] used two mean-field homogenization methods, namely the Mori-Tanaka scheme and the double inclusion model (see Fig. 17), to predict the stiffness properties of activated fly ash pastes. The Mori-Tanaka approach provided slightly higher values because it does not take into account the interactions between the different inclusions. Conversely, the results obtained using the double inclusion method were found to be close to the experimental stiffness values as it more

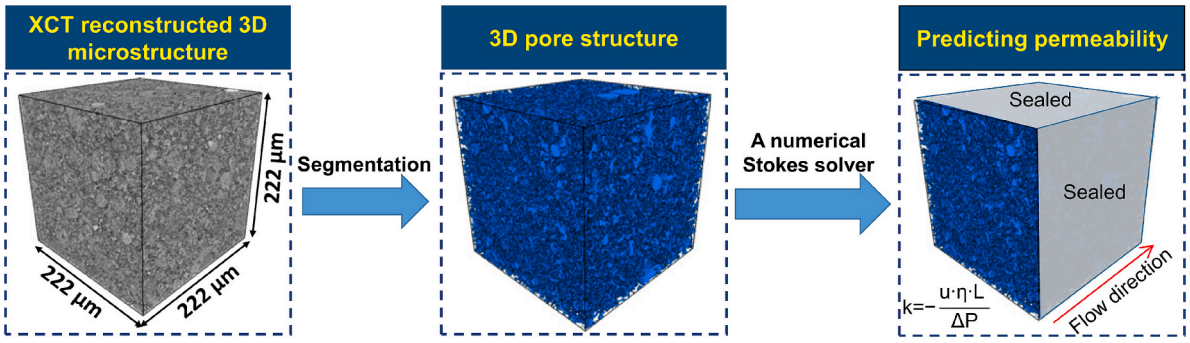

Fig. 16. Predicting permeability of alkali-activated fly ash from its X-ray tomography reconstructed 3D microstructure [145].

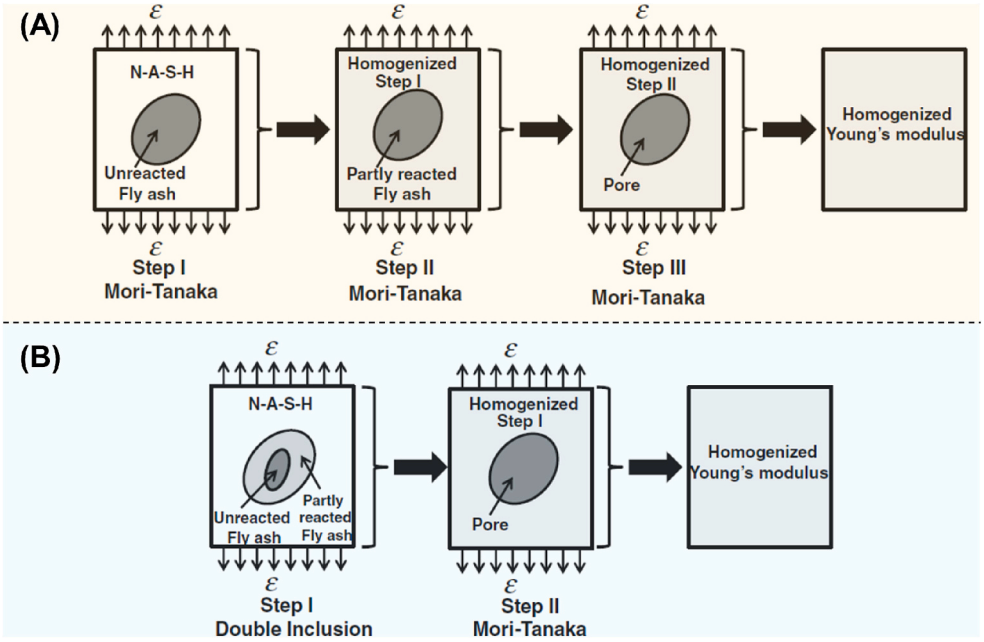

Fig. 17. Representation of two homogenization process method: (A) Mori-Tanaka method, and (B) double inclusion method [145].

accurately represents the heterogeneity of the material. It should be noted that the Mori-Tanaka scheme may be more computationally efficient for simple microstructures, while the double inclusion model may provide better accuracy for more complex heterogeneous materials, such as AAMs. Königsberger et al. [163] proposed an image-supported grid nanoindentation method to determine the elastic phase stiffness of AAM. In order to validate this new testing protocol, homogenization theory based on Hashin-Shtrikman bounds was used to upscale the nanoindentation moduli to bounds for the ultrasonic wave velocities for AAM, showing a good agreement.

Fang and Zhang [164] also used micromechanics to correlate micromechanical properties obtained from nanoindentation testing with the macroscopic elasticity of alkali-activated fly ash-slag pastes. The material was represented by three consecutively arranged representative volume elements (RVE) at the solid gel particle, gel matrix and paste levels, in analogy to Šmilauer et al. [162]. The effective mechanical properties of the AAFS paste were calculated using the self-consistent scheme considering only spherical material phases. The authors were able to show that the mechanical behavior of the paste is mainly determined by the micromechanical properties of the reaction products at the smallest observed scale and their volume fractions. However, the effective mechanical properties that were calculated using homogenization theory do not change with time, which is not reasonable in the context of an ongoing reaction between the precursors and the alkaline activating solution.

In another study, homogenization theory was also applied by Caron et al. [165] to evaluate the Young's modulus of alkali-activated slag concrete. A five-step analytical model up to the concrete scale was proposed as shown in Fig. 18. The evolution of the phase volume fractions as a function of the time was obtained from thermodynamic modeling. A comparison of modeled and experimental stiffness values at the paste level showed a very good agreement. A model accuracy of 95% was claimed for the Young's modulus at 28 days. Notably, the authors considered the ITZ around the sand grains at the level of mortar directly in their model, but their studies related to the effects of the thickness of the ITZ showed that it can be neglected in future calculations. Sensitivity analyses with several parameters indicate that the activator solution has an even greater influence on the modeled engineering properties than the composition of the slag.

Although several successful studies have already been published, future and more detailed work is required. This applies to the morphological representation of the alkali-activated materials. So far, the material phases in published models are represented by spheres, whereas the actual microstructures of AAMs contain angular particles as important contributors on many length scales (e.g. plate-shaped hydrate particles, remnant slag grains, and angular sand particles). In addition, the micromechanical approaches should be extended to predict other mechanical properties, such as time-dependent creep and shrinkage,

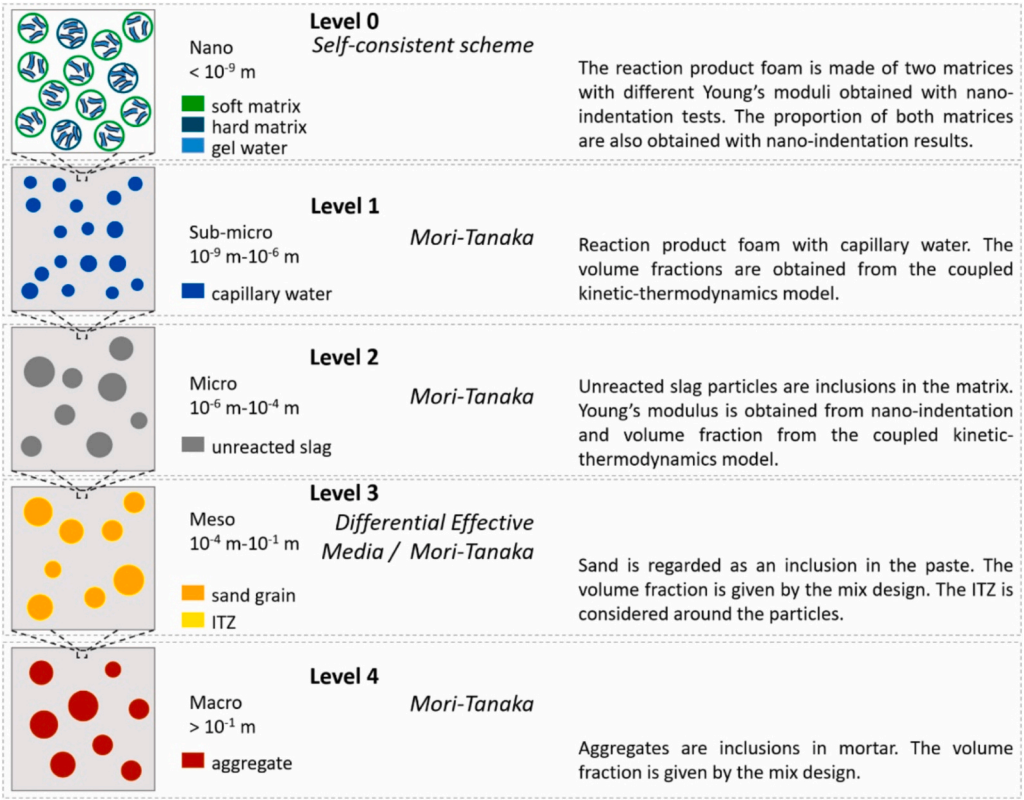

Fig. 18. A five-step homogenization scheme [165].

which are controlled to a significant extent by capillary-scale processes.

Some recent studies have also applied advanced numerical techniques, such as Discrete Element Method (DEM) and Finite Element Method (FEM) approaches, to model the multiscale structure and properties of AAMs [166,167]. These physics-based modeling approaches can provide additional insight into the complex microstructural interactions in composite materials such as AAMs. Nguyen et al. [168] used DEM to investigate the effects of pore-structure and mortar properties on the fracture behavior of foamed geopolymer concrete (see Fig. 19). Their numerical results show that the porosity and pore size distribution can have a profound effect on the fracture resistance of the material and that the fracture process exhibits a gradual transition contact bonds from compressive to tensile modes as the loading progresses. Caggiano et al. [169] proposed an upscaling procedure to model the thermal energy storage (TES) properties of geopolymer pastes, where an atomistic approach was used to model the thermal behavior and heat storage capacity of N-A-S-H gels, and then an up-scaling optimization procedure and *meso*-scale FEM homogenization techniques were used to link the TES parameters of N-A-S-H gels to the homogenized upper meso/macro scale values. The simulation results demonstrated a good agreement with the experimental data in terms of heat capacity and thermal diffusivity. However, computational cost may be a limitation for large-scale FEM simulations. Therefore, more efficient algorithms and upscaling techniques may be needed in this regard.

Overall, the existing literature shows promising progress in multiscale modeling of AAMs, but there are still challenges in accurately representing the hierarchical structures and interactions as well as linking chemistry to mechanical/thermal properties. In addition, the computational requirements for implementing such modeling approaches are still substantial. Further efforts are also needed to develop comprehensive and efficient multiscale models to incorporate coupled chemo-thermal-mechanical effects in AAMs. Simulations of the long-term properties of AAMs, such as shrinkage and transport properties, has received little attention and should therefore be given greater consideration. However, it is expected that these aspects will continue to develop in the upcoming years, via improvement of both theoretical

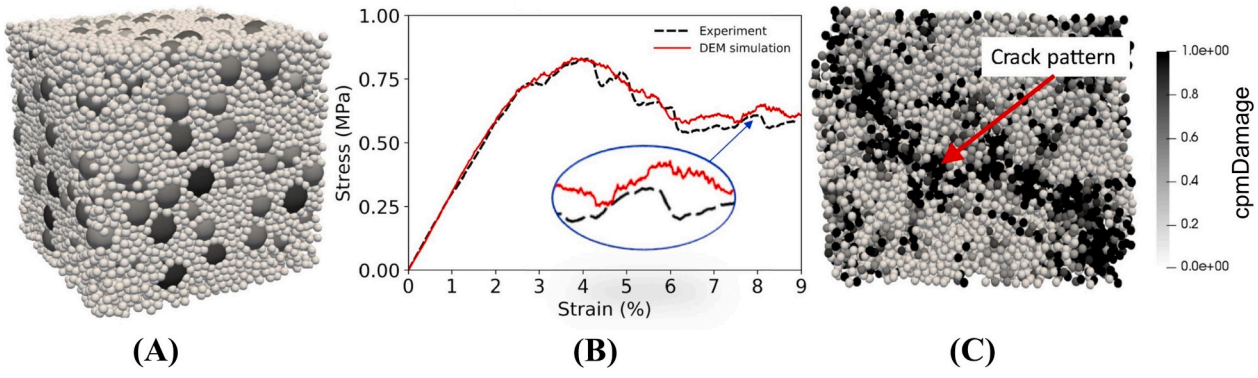

Fig. 19. (A) DEM modeling of foamed geopolymer concrete, (B) stress-strain curves and (C) crack pattern of the calibrated DEM model [168].

explanations of AAM chemistry, coupling mechanisms and the accessibility of computational capabilities.

6. Conclusions and perspectives

Over the last two decades, pioneering work has been carried out on the modeling and simulation of AAMs, yielding fruitful results. Atomistic simulations of C-(N-)A-S-H and N-A-S-H gels have provided valuable insights into their structure and composition, and intrinsic mechanical and transport-related properties. Thermodynamic modeling can reveal the phase evolution and durability of AAMs with the cause of chemical reactions. By combining thermodynamics and kinetics, the GeoMicro3D model simulates the microstructure formation of AAMs resulting from the continuous formation of reaction products, providing a solid foundation for conducting numerical studies on the microstructure-related properties, such as tensile strength, permeability, and diffusivity of chloride. The macroscopic properties of AAMs are related to their hierarchical structures, interactions and binder chemistry. Multiscale modeling, which is an accepted modeling strategy, shows promising potential in predicting the mechanical properties and fracture property as well as other macroscopic properties of AAMs. In the future, more attention should be paid to the following aspects of modeling and simulation of AAMs:

- Atomistic models are usually developed separately to reproduce the molecular mechanisms and properties of C-(N-)A-S-H and N-A-S-H gels for alkali activated high-Ca and low-Ca AAMs, respectively. There is a lack of atomistic modeling work devoted to blends of C-(N-)A-S-H and N-A-S-H gels and exploring their interaction mechanisms for alkali activated medium-Ca AAMs. Besides, the atomistic simulation results mostly lack experimental data to validate them, and the upscaling method from these atomistic simulation results to macroscale application remains largely implicit.
- The thermodynamic database is well developed for AAMs with high-Ca content, but it is still underdeveloped for AAMs with low to none calcium, and for high-Fe phases, which limits the application of thermodynamic modeling to AAMs. Although the N(*C*)ASH_ss model for the description of the N-A-S-H gel has been developed and implemented in the thermodynamic modeling of low-Ca and medium-Ca AAMs, it is desirable to develop a thermodynamic model from a mechanistic point of view via atomistic simulation.
- Many properties are dependent on the microstructure of AAMs, but there are few numerical models available and suitable for simulating the microstructure formation of AAMs as compared to those developed for PC-based materials. GeoMicro3D has been developed for the first time to simulate the reaction process and microstructure formation of AAMs, but it still needs further development and verification.
- At present, only a few researchers have focused on the microstructure-based and multiscale modeling of AAMs, mainly using analytical homogenization theory. Future studies in this field may focus on introducing different phase shapes and on extending the applicability of these models. For predicting the durability of various AAMs that cover e.g. transport of ions or aggressive media, numerical models that take into account the spatial structure of AAMs should be established.

CRediT authorship contribution statement

Yibing Zuo: Writing – review & editing, Writing – original draft, Methodology, Investigation, Funding acquisition, Formal analysis, Conceptualization. **Yun Chen:** Writing – review & editing, Writing – original draft, Formal analysis. **Chen Liu:** Writing – review & editing, Writing – original draft, Formal analysis. **Yidong Gan:** Writing – review & editing, Writing – original draft, Formal analysis. **Luise Göbel:** Writing – review & editing, Writing – original draft, Formal analysis. **Guang Ye:** Writing – review & editing, Resources, Conceptualization. **John L. Provis:** Writing – review & editing, Supervision, Formal analysis.

Declaration of competing interest

The authors declare no conflict of interest.

Acknowledgements

Y Zuo would like to gratefully acknowledge the National Key Research and Development Program of China [grant number 2023YFC3902802] and the Fundamental Research Funds for the Natural Science Foundation of Hubei Province [grant numbers 2022CFB048, 2024AFB562].

Data availability

Data will be made available on request.

References

[1] P.S. Deb, P. Nath, P.K. Sarker, The effects of ground granulated blast-furnace slag blending with fly ash and activator content on the workability and strength properties of geopolymer concrete cured at ambient temperature, Mater. Des. 62 (2014) 32–39.
[2] H. Ye, Z. Chen, L. Huang, Mechanism of sulfate attack on alkali-activated slag: the role of activator composition, Cem. Concr. Res. 125 (2019) 105868.
[3] Z. Li, M. Nedeljković, B. Chen, G. Ye, Mitigating the autogenous shrinkage of alkali-activated slag by metakaolin, Cem. Concr. Res. 122 (2019) 30–41.
[4] P.K. Sarker, S. Kelly, Z. Yao, Effect of fire exposure on cracking, spalling and residual strength of fly ash geopolymer concrete, Mater. Des. 63 (2014) 584–592.
[5] J.L. Provis, Alkali-activated materials, Cem. Concr. Res. 114 (2018) 40–48.
[6] C. Shi, B. Qu, J.L. Provis, Recent progress in low-carbon binders, Cem. Concr. Res. 122 (2019) 227–250.
[7] J.S. van Deventer, C.E. White, R.J. Myers, A roadmap for production of cement and concrete with low-CO 2 emissions, Waste Biomass Valori. 12 (2021) 4745–4775.
[8] J.S. Dolado, K. van Breugel, Recent advances in modeling for cementitious materials, Cem. Concr. Res. 41 (2011) 711–726.
[9] J.J. Thomas, J.J. Biernacki, J.W. Bullard, S. Bishnoi, J.S. Dolado, G.W. Scherer, A. Luttge, Modeling and simulation of cement hydration kinetics and microstructure development, Cem. Concr. Res. 41 (2011) 1257–1278.
[10] K.v. Breugel, Simulation of Hydration and Formation of Structure in Hardening Cement-Based Materials, PhD, Delft University of Technology, 1991.
[11] D.P. Bentz, Three-dimensional computer simulation of Portland cement hydration and microstructure development, J. Am. Ceram. Soc. 80 (1997) 3–21.
[12] Z. Giergiczny, Fly ash and slag, Cem. Concr. Res. 124 (2019) 105826.
[13] J.L. Provis, S.A. Bernal, Geopolymers and related alkali-activated materials, Annu. Rev. Mater. Res. 44 (2014) 299–327.
[14] J.S.J. van Deventer, J.L. Provis, P. Duxson, Technical and commercial progress in the adoption of geopolymer cement, Miner. Eng. 29 (2012) 89–104.
[15] C. Li, H.H. Sun, L.T. Li, A review: the comparison between alkali-activated slag (Si plus ca) and metakaolin (Si plus Al) cements, Cem. Concr. Res. 40 (2010) 1341–1349.
[16] S. Puligilla, P. Mondal, Co-existence of aluminosilicate and calcium silicate gel characterized through selective dissolution and FTIR spectral subtraction, Cem. Concr. Res. 70 (2015) 39–49.
[17] J.L. Provis, G.C. Lukey, J.S.J. van Deventer, Do geopolymers actually contain nanocrystalline zeolites? A reexamination of existing results, Chem. Mater. 17 (2005) 3075–3085.
[18] M.R. Rowles, B.H. O'Connor, Chemical and structural microanalysis of aluminosilicate geopolymers synthesized by sodium silicate activation of metakaolinite, J. Am. Ceram. Soc. 92 (2009) 2354–2361.
[19] F. Pacheco-Torgal, J. Labrincha, C. Leonelli, A. Palomo, P. Chindaprasit, Handbook of Alkali-Activated Cements, Mortars and Concretes, Elsevier, 2014.
[20] X. Dai, S. Aydin, M.Y. Yardimci, K. Lesage, G. De Schutter, Early age reaction, rheological properties and pore solution chemistry of NaOH-activated slag mixtures, Cem. Concr. Compos. 133 (2022) 104715.
[21] Y. Zuo, M. Nedeljković, G. Ye, Pore solution composition of alkali-activated slag/fly ash pastes, Cem. Concr. Res. 115 (2019) 230–250.
[22] D. Jiang, Z. Zhang, C. Shi, Evolution of silicate species from waterglass in waterglass activated slag (WAS) pastes at early age, Cem. Concr. Res. 180 (2024) 107513.
[23] F. Puertas, A. Fernández-Jiménez, M.T. Blanco-Varela, Pore solution in alkali-activated slag cement pastes. Relation to the composition and structure of calcium silicate hydrate, Cem. Concr. Res. 34 (2004) 139–148.
[24] R.J. Myers, S.A. Bernal, J.L. Provis, Phase diagrams for alkali-activated slag binders, Cem. Concr. Res. 95 (2017) 30–38.

[25] M. Ben Haha, G. Le Saout, F. Winnefeld, B. Lothenbach, Influence of activator type on hydration kinetics, hydrate assemblage and microstructural development of alkali activated blast-furnace slags, Cem. Concr. Res. 41 (2011) 301–310.
[26] Y. Ma, J. Hu, G. Ye, The effect of activating solution on the mechanical strength, reaction rate, mineralogy, and microstructure of alkali-activated fly ash, J. Mater. Sci. 47 (2012) 4568–4578.
[27] Z. Zhang, R. Chen, J. Hu, Y. Wang, H. Huang, Y. Ma, Z. Zhang, H. Wang, S. Yin, J. Wei, Q. Yu, Corrosion behavior of the reinforcement in chloride-contaminated alkali-activated fly ash pore solution, Compos. Part B 224 (2021) 109215.
[28] V.O. Ozçelik, C.E. White, Nanoscale charge-balancing mechanism in alkali-substituted calcium–silicate–hydrate gels, J. Phys. Chem. Lett. 7 (2016) 5266–5272.
[29] Y. Zuo, L. Göbel, J. Yliniemi, J.L. Provis, Chapter 5 Modelling and Simulation of Alkali Activated Materials, State-of-the-art report of TC MPA on alkali-activated materials, 2024.
[30] A. Özbayrak, H. Kucukgoncu, O. Atas, H.H. Aslanbay, Y.G. Aslanbay, F. Altun, Determination of stress-strain relationship based on alkali activator ratios in geopolymer concretes and development of empirical formulations, Struct 48 (2023) 2048–2061.
[31] B. Sun, L. Ding, G. Ye, G. De Schutter, Mechanical properties prediction of blast furnace slag and fly ash-based alkali-activated concrete by machine learning methods, Constr. Build. Mater. 409 (2023) 133933.
[32] A. Nazari, J.G. Sanjayan, Modelling of compressive strength of geopolymer paste, mortar and concrete by optimized support vector machine, Ceram. Int. 41 (2015) 12164–12177.
[33] R.J. Myers, S.A. Bernal, R. San Nicolas, J.L. Provis, Generalized structural description of calcium–sodium aluminosilicate hydrate gels: the cross-linked substituted tobermorite model, Langmuir 29 (2013) 5294–5306.
[34] M.B. Haha, B. Lothenbach, G. Le Saout, F. Winnefeld, Influence of slag chemistry on the hydration of alkali-activated blast-furnace slag — part I: effect of MgO, Cem. Concr. Res. 41 (2011) 955–963.
[35] M.B. Haha, B. Lothenbach, G. Le Saout, F. Winnefeld, Influence of slag chemistry on the hydration of alkali-activated blast-furnace slag — part II: effect of Al2O3, Cem. Concr. Res. 42 (2012) 74–83.
[36] R.J. Myers, S.A. Bernal, J.D. Gehman, J.S. Deventer, J.L. Provis, The role of Al in cross-linking of alkali-activated slag cements, J. Am. Ceram. Soc. 996-1004 (2015).
[37] M.J. Abdolhosseini Qomi, F.-J. Ulm, R.J.-M. Pellenq, Evidence on the dual nature of aluminum in the calcium-silicate-hydrates based on atomistic simulations, J. Am. Ceram. Soc. 95 (2012) 1128–1137.
[38] C.E. White, L.L. Daemen, M. Hartl, K. Page, Intrinsic differences in atomic ordering of calcium (alumino)silicate hydrates in conventional and alkali-activated cements, Cem. Concr. Res. 67 (2015) 66–73.
[39] J. Yang, D. Hou, Q. Ding, Structure, dynamics, and mechanical properties of cross-linked calcium Aluminosilicate hydrate: a molecular dynamics study, ACS Sustain. Chem. Eng. 6 (2018) 9403–9417.
[40] X. Wan, D. Hou, T. Zhao, L. Wang, Insights on molecular structure and micro-properties of alkali-activated slag materials: a reactive molecular dynamics study, Constr. Build. Mater. 139 (2017) 430–437.
[41] D. Hou, C. Wu, Q. Yang, W. Zhang, Z. Lu, P. Wang, J. Li, Q. Ding, Insights on the molecular structure evolution for tricalcium silicate and slag composite: from 29Si and 27Al NMR to molecular dynamics, Compos. Part B 202 (2020) 108401.
[42] S. Zhang, E. Duque-Redondo, A. Kostiuchenko, J.S. Dolado, G. Ye, Molecular dynamics and experimental study on the adhesion mechanism of polyvinyl alcohol (PVA) fiber in alkali-activated slag/fly ash, Cem. Concr. Res. 145 (2021) 106452.
[43] D. Hou, T. Li, P. Wang, Molecular dynamics study on the structure and dynamics of NaCl solution transport in the Nanometer Channel of CASH gel, ACS Sustain. Chem. Eng. 6 (2018) 9498–9509.
[44] D. Hou, T. Li, Influence of aluminates on the structure and dynamics of water and ions in the nanometer channel of calcium silicate hydrate (C–S–H) gel, Phys. Chem. Chem. Phys. 20 (2018) 2373–2387.
[45] X. Liu, P. Feng, W. Li, G. Geng, J. Huang, Y. Gao, S. Mu, J. Hong, Effects of pH on the nano/micro structure of calcium silicate hydrate (C-S-H) under sulfate attack, Cem. Concr. Res. 140 (2021) 106306.
[46] Q. Ding, J. Yang, D. Hou, G. Zhang, Insight on the mechanism of sulfate attacking on the cement paste with granulated blast furnace slag: an experimental and molecular dynamics study, Constr. Build. Mater. 169 (2018) 601–611.
[47] H. Manzano, J. Dolado, M. Griebel, J. Hamaekers, A molecular dynamics study of the aluminosilicate chains structure in Al-rich calcium silicate hydrated (C–S–H) gels, Phys. Status Solidi A 205 (2008) 1324–1329.
[48] F. Puertas, M. Palacios, H. Manzano, J.S. Dolado, A. Rico, J. Rodríguez, A model for the C-A-S-H gel formed in alkali-activated slag cements, J. Eur. Ceram. Soc. 31 (2011) 2043–2056.
[49] S.V. Churakov, C. Labbez, Thermodynamics and molecular mechanism of Al incorporation in calcium silicate hydrates, J. Phys. Chem. C 121 (2017) 4412–4419.
[50] A. Rawal, B.J. Smith, G.L. Athens, C.L. Edwards, L. Roberts, V. Gupta, B. F. Chmelka, Molecular silicate and aluminate species in anhydrous and hydrated cements, J. Am. Chem. Soc. 132 (2010) 7321–7337.
[51] N. Garg, V.O. Özçelik, J. Skibsted, C.E. White, Nanoscale ordering and Depolymerization of calcium silicate hydrates in the presence of alkalis, J. Phys. Chem. C 123 (2019) 24873–24883.
[52] R.J. Myers, E. L'Hôpital, J.L. Provis, B. Lothenbach, Effect of temperature and aluminium on calcium (alumino) silicate hydrate chemistry under equilibrium conditions, Cem. Concr. Res. 68 (2015) 83–93.
[53] K.C. Reddy, K.V.L. Subramaniam, Investigation on the roles of solution-based alkali and silica in activated low-calcium fly ash and slag blends, Cem. Concr. Compos. 123 (2021) 104175.
[54] C. Liu, X. Liang, Y. Chen, Z. Li, G. Ye, Degradation of alkali-activated slag subjected to water immersion, Cem. Concr. Compos. 142 (2023) 105157.
[55] C. Liu, Z. Li, S. Nie, J. Skibsted, G. Ye, Structural evolution of calcium sodium aluminosilicate hydrate (C-(N-)A-S-H) gels induced by water exposure: the impact of Na leaching, Cem. Concr. Res. 178 (2024) 107432.
[56] L.-Y. Xu, Y. Alrefaei, Y.-S. Wang, J.-G. Dai, Recent advances in molecular dynamics simulation of the N-A-S-H geopolymer system: modeling, structural analysis, and dynamics, Constr. Build. Mater. 276 (2021) 122196.
[57] M. Zhang, N.A. Deskins, G. Zhang, R.T. Cygan, M. Tao, Modeling the polymerization process for Geopolymer synthesis through reactive molecular dynamics simulations, J. Phys. Chem. C 122 (2018) 6760–6773.
[58] Y. Chen, J. S. Dolado, Z. Li, S. Yin, Q. Yu, A. Kostiuchenko, G. Ye, A molecular dynamics study of N–A–S–H gel with various Si/Al ratios, J. Am. Ceram. Soc. 105 (2022) 18597.
[59] D. Hou, F. Hong, B. Dong, P. Wang, Y. Zhang, X. Wang, M. Wang, Molecular insights into the reaction process of alkali-activated Metakaolin by sodium hydroxide, Langmuir 38 (2022) 11337–11345.
[60] F. Lolli, H. Manzano, J.L. Provis, M.C. Bignozzi, E. Masoero, Atomistic simulations of geopolymer models: the impact of disorder on structure and mechanics, ACS Appl. Mater. Interfaces 22809-22820 (2018).
[61] M.R. Sadat, S. Bringuier, K. Muralidharan, K. Runge, A. Asaduzzaman, L. Zhang, An atomistic characterization of the interplay between composition, structure and mechanical properties of amorphous geopolymer binders, J. Non-Cryst. Solids 434 (2016) 53–61.
[62] R. Wang, J. Wang, T. Dong, G. Ouyang, Structural and mechanical properties of geopolymers made of aluminosilicate powder with different SiO2/Al2O3 ratio: molecular dynamics simulation and microstructural experimental study, Constr. Build. Mater. 240 (2020) 117935.
[63] Y. Zhang, J. Zhang, J. Jiang, D. Hou, J. Zhang, The effect of water molecules on the structure, dynamics, and mechanical properties of sodium aluminosilicate hydrate (NASH) gel: a molecular dynamics study, Constr. Build. Mater. 193 (2018) 491–500.
[64] M.R. Sadat, S. Bringuier, A. Asaduzzaman, K. Muralidharan, L. Zhang, A molecular dynamics study of the role of molecular water on the structure and mechanics of amorphous geopolymer binders, J. Chem. Phys. 145 (2016) 134706.
[65] X. Guan, L. Jiang, D. Fan, A. Garcia Hernandez, B. Li, H. Do, Molecular simulations of the structure-property relationships of N-A-S-H gels, Constr. Build. Mater. 329 (2022) 127166.
[66] Z. Li, J. Zhang, M. Wang, Structure, reactivity, and mechanical properties of sustainable Geopolymer material: a reactive molecular dynamics study, Front. Mater. 7 (2020) 69.
[67] G.A. Lyngdoh, S. Nayak, N.M.A. Krishnan, S. Das, Fracture toughness of fly ash-based geopolymer gels: evaluations using nanoindentation experiment and molecular dynamics simulation, Constr. Build. Mater. 262 (2020) 120797.
[68] G.A. Lyngdoh, R. Kumar, N.M.A. Krishnan, S. Das, Dynamics of confined water and its interplay with alkali cations in sodium aluminosilicate hydrate gel: insights from reactive force field molecular dynamics, Phys. Chem. Chem. Phys. 22 (2020) 23707–23724.
[69] Y. Zhang, T. Li, D. Hou, J. Zhang, J. Jiang, Insights on magnesium and sulfate ions' adsorption on the surface of sodium alumino-silicate hydrate (NASH) gel: a molecular dynamics study, Phys. Chem. Chem. Phys. 20 (2018) 18297–18310.
[70] D. Hou, J. Zhang, W. Pan, Y. Zhang, Z. Zhang, Nanoscale mechanism of ions immobilized by the geopolymer: a molecular dynamics study, J. Nucl. Mater. 528 (2020) 151841.
[71] A. Bagheri, A. Nazari, J.G. Sanjayan, W. Duan, Molecular simulation of water and chloride ion diffusion in nanopores of alkali-activated aluminosilicate structures, Ceram. Int. 44 (2018) 20723–20731.
[72] D. Hou, Y. Zhang, T. Yang, J. Zhang, H. Pei, J. Zhang, J. Jiang, T. Li, Molecular structure, dynamics, and mechanical behavior of sodium aluminosilicate hydrate (NASH) gel at elevated temperature: a molecular dynamics study, Phys. Chem. Chem. Phys. 20 (2018) 20695–20711.
[73] W. Zhang, J.-s. Li, X. Huang, Z. Chen, L. Lang, K. Huang, Unraveling the cation adsorption of geopolymer binder: a molecular dynamics study, Chemosphere 335 (2023) 139118.
[74] G.A. Lyngdoh, S. Nayak, R. Kumar, N.M. Anoop Krishnan, S. Das, Fracture toughness of sodium aluminosilicate hydrate (NASH) gels: insights from molecular dynamics simulations, J. Appl. Phys. 127 (2020).
[75] G.A. Lyngdoh, R. Kumar, N.M.A. Krishnan, S. Das, Realistic atomic structure of fly ash-based geopolymer gels: insights from molecular dynamics simulations, J. Chem. Phys. 151 (2019) 064307.
[76] M.R. Sadat, S. Bringuier, K. Muralidharan, G. Frantziskonis, L. Zhang, Atomic-scale dynamics and mechanical response of geopolymer binder under nanoindentation, Comput. Mater. Sci. 142 (2018) 227–236.
[77] X. Guan, J.-Q. Wu, A.G. Hernandez, B. Li, H. Do, Molecular dynamic simulations of interfacial interaction mechanism between the NASH gels and the polyethene fibre, Constr. Build. Mater. 349 (2022) 128769.
[78] D. Damidot, B. Lothenbach, D. Herfort, F.P. Glasser, Thermodynamics and cement science, Cem. Concr. Res. 41 (2011) 679–695.
[79] R.A. Van Santen, The Ostwald step rule, J. Phys. Chem. 88 (1984) 5768–5769.
[80] I. Ismail, S.A. Bernal, J.L. Provis, R.S. Nicolas, S. Hamdan, J.S.J. van Deventer, Modification of phase evolution in alkali-activated blast furnace slag by the incorporation of fly ash, Cem. Concr. Compos. 45 (2014) 125–135.

[81] S.A. Bernal, J.L. Provis, B. Walkley, R. San Nicolas, J.D. Gehman, D.G. Brice, A. R. Kilcullen, P. Duxson, J.S. van Deventer, Gel nanostructure in alkali-activated binders based on slag and fly ash, and effects of accelerated carbonation, Cem. Concr. Res. 53 (2013) 127–144.

[82] R.J. Myers, S.A. Bernal, J.L. Provis, A thermodynamic model for C-(N-)A-S-H gel: CNASH_ss. Derivation and validation, Cem. Concr. Res. 66 (2014) 27–47.

[83] R.J. Myers, B. Lothenbach, S.A. Bernal, J.L. Provis, Thermodynamic modelling of alkali-activated slag cements, Appl. Geochem. 61 (2015) 233–247.

[84] G.D. Miron, D.A. Kulik, Y. Yan, J. Tits, B. Lothenbach, Extensions of CASH+ thermodynamic solid solution model for the uptake of alkali metals and alkaline earth metals in C-S-H, Cem. Concr. Res. 152 (2022) 106667.

[85] B. Lothenbach, D.A. Kulik, T. Matschei, M. Balonis, L. Baquerizo, B. Dilnesa, G. D. Miron, R.J. Myers, Cemdata18: a chemical thermodynamic database for hydrated Portland cements and alkali-activated materials, Cem. Concr. Res. 115 (2019) 472–506.

[86] Y. Chen, L.M. de Lima, Z. Li, B. Ma, B. Lothenbach, S. Yin, Q. Yu, G. Ye, Synthesis, solubility and thermodynamic properties of N-A-S-H gels with various target Si/Al ratios, Cem. Concr. Res. 180 (2024) 107484.

[87] B. Walkley, X. Ke, O. Hussein, J.L. Provis, Thermodynamic properties of sodium aluminosilicate hydrate (N–A–S–H), Dalton T 50 (2021) 13968–13984.

[88] L. Gomez-Zamorano, M. Balonis, B. Erdemli, N. Neithalath, G. Sant, C–(N)–S–H and N–A–S–H gels: Compositions and solubility data at 25 °C and 50 °C, J. Am. Ceram. Soc. 100 (2017) 2700–2711.

[89] B. Lothenbach, E. Bernard, U. Mäder, Zeolite formation in the presence of cement hydrates and albite, Phys. Chem. Earth 99 (2017) 77–94.

[90] B. Ma, B. Lothenbach, Thermodynamic study of cement/rock interactions using experimentally generated solubility data of zeolites, Cem. Concr. Res. 135 (2020) 106149.

[91] B. Ma, B. Lothenbach, Synthesis, characterization, and thermodynamic study of selected K-based zeolites, Cem. Concr. Res. 148 (2021) 106537.

[92] C.E. White, J.L. Provis, T. Proffen, J.S. Van Deventer, The effects of temperature on the local structure of metakaolin-based geopolymer binder: a neutron pair distribution function investigation, J. Am. Ceram. Soc. 93 (2010) 3486–3492.

[93] J.L. Bell, P. Sarin, P.E. Driemeyer, R.P. Haggerty, P.J. Chupas, W.M. Kriven, X-ray pair distribution function analysis of a metakaolin-based, KAlSi 2 O 6· 5.5 H 2 O inorganic polymer (geopolymer), J. Mater. Chem. 18 (2008) 5974–5981.

[94] J. Davidovits, Geopolymers, J. Therm. Anal. 37 (1991) 1633–1656.

[95] Z. Zuhua, Y. Xiao, Z. Huajun, C. Yue, Role of water in the synthesis of calcined kaolin-based geopolymer, Appl. Clay Sci. 43 (2009) 218–223.

[96] Y. Zuo, Experimental Study and Numerical Simulation of the Reaction Process and Microstructure Formation of Alkali-Activated Materials, PhD thesis,, Delft University of Technology, 2019.

[97] I. García-Lodeiro, A. Fernández-Jiménez, A. Palomo, D. E. Macphee, Effect of calcium additions on N–A–S–H cementitious gels, J. Am. Ceram. Soc. 93 (2010) 1934–1940.

[98] A. Peys, V. Isteri, J. Yliniemi, A.S. Yorkshire, P.N. Lemougna, C. Utton, J.L. Provis, R. Snellings, T. Hanein, Sustainable iron-rich cements: raw material sources and binder types, Cem. Concr. Res. 157 (2022) 106834.

[99] Y. Fang, K. Zhuang, H. Cui, Z. Zhang, A. Wang, C. Wang, D. Zheng, X. Wang, The state of Fe3+ in the C–F–A–S–H system with varying Fe/Si and Ca/Si ratios, J. Mater. Chem. A 11 (2023) 26193–26211.

[100] A. Baral, C. Pesce, A.S. Yorkshire, Z. Zhakiyeva, R. Snellings, T. Hanein, J. L. Provis, A. Peys, Characterisation of iron-rich cementitious materials, Cem. Concr. Res. 177 (2024) 107419.

[101] M. Zhang, E. Bernard, M.H.N. Yio, C.R. Cheeseman, R.J. Myers, Synthesis of Sodium iron Silicate Hydrate (N-F-S-H), in: Proceedings of the 16th International Congress on the Chemistry of Cement, Bangkok, Thailand, 2023.

[102] S. Ghazizadeh, T. Hanein, J.L. Provis, T. Matschei, Estimation of standard molar entropy of cement hydrates and clinker minerals, Cem. Concr. Res. 136 (2020) 106188.

[103] D.A. Kulik, T. Wagner, S.V. Dmytrieva, G. Kosakowski, F.F. Hingerl, K. V. Chudnenko, U.R. Berner, GEM-Selektor geochemical modeling package: revised algorithm and GEMS3K numerical kernel for coupled simulation codes, Comput. Geosci. 17 (2013) 1–24.

[104] T. Wagner, D.A. Kulik, F.F. Hingerl, S.V. Dmytrieva, GEM-Selektor geochemical modeling package: TSolMod library and data interface for multicomponent phase models, Can. Mineral. 50 (2012) 1173–1195.

[105] D.L. Parkhurst, C. Appelo, Description of input and examples for PHREEQC version 3—a computer program for speciation, batch-reaction, one-dimensional transport, and inverse geochemical calculations, US geological survey techniques and methods 6 (2013) 497.

[106] B. Lothenbach, T. Matschei, G. Möschner, F.P. Glasser, Thermodynamic modelling of the effect of temperature on the hydration and porosity of Portland cement, Cem. Concr. Res. 38 (2008) 1–18.

[107] D.A. Kulik, Minimising Uncertainty Induced by Temperature Extrapolations of Thermodynamic Data: A Pragmatic View on the Integration of Thermodynamic Databases into Geochemical Computer Codes, in: F, Monpean, Proceedings of The use of thermodynamic databases in performance assessment, Barcelona, Spain, 2002.

[108] B. Lothenbach, Thermodynamic equilibrium calculations in cementitious systems, Mater. Struct. 43 (2010) 1413–1433.

[109] B. Lothenbach, A. Gruskovnjak, Hydration of alkali-activated slag: thermodynamic modelling, Adv. Cem. Res. 19 (2007) 81–92.

[110] K.S. Pitzer, Ion Interaction Approach: Theory and Data Correlation, Activity Coefficients in Electrolyte Solutions, CRC Press, Roca Raton, 1991.

[111] K.S. Pitzer, A thermodynamic model for aqueous solutions of liquid-like density, Rev. Mineral. Geochem. 17 (1987) 97–142.

[112] R. Caron, R.A. Patel, G.D. Miron, C. Le Galliard, B. Lothenbach, F. Dehn, Microstructure development of slag activated with sodium silicate solution: experimental characterization and thermodynamic modeling, J. Build. Eng. 71 (2023) 106398.

[113] O. Burciaga-Díaz, J.I. Escalante-García, Structure, mechanisms of reaction, and strength of an alkali-activated blast-furnace slag, J. Am. Ceram. Soc. 96 (2013) 3939–3948.

[114] S.A. Bernal, R. San Nicolas, R.J. Myers, R. Mejía de Gutiérrez, F. Puertas, J.S. J. van Deventer, J.L. Provis, MgO content of slag controls phase evolution and structural changes induced by accelerated carbonation in alkali-activated binders, Cem. Concr. Res. 57 (2014) 33–43.

[115] H. Ye, A. Radlińska, Quantitative analysis of phase assemblage and chemical shrinkage of alkali-activated slag, J. Adv. Concr. Technol. 14 (2016) 245–260.

[116] Y. Zuo, M. Nedeljković, G. Ye, Coupled thermodynamic modelling and experimental study of sodium hydroxide activated slag, Constr. Build. Mater. 188 (2018) 262–279.

[117] X. Ke, S.A. Bernal, J.L. Provis, B. Lothenbach, Thermodynamic modelling of phase evolution in alkali-activated slag cements exposed to carbon dioxide, Cem. Concr. Res. 136 (2020) 106158.

[118] Y. Zuo, Effect of chloride salt on the phase evolution in alkali-activated slag cements through thermodynamic modelling, Appl. Geochem. 136 (2022) 105169.

[119] Y. Zuo, Thermodynamic modeling of the phase evolution in alkali-activated slag cements with sulfate salt exposure, J. Am. Ceram. Soc. 105 (2022) 18661.

[120] K.C. Reddy, G.M. Kim, S. Park, Modeling the phase evolution in alkali-activated slag cements upon interaction with seawater, Case Stud. Constr. Mater. 17 (2022) e01476.

[121] Y. Zuo, Y. Liao, G. Ye, Thermodynamic modelling of phase evolution in alkali-activated slag cement upon combined attack of salt, J. Build. Mater. 26 (2023) 7–13 (in Chinese).

[122] S. Mundra, D.P. Prentice, S.A. Bernal, J.L. Provis, Modelling chloride transport in alkali-activated slags, Cem. Concr. Res. 130 (2020) 106011.

[123] Y. Chen, B. Ma, J. Chen, Z. Li, X. Liang, L.M. de Lima, C. Liu, S. Yin, Q. Yu, B. Lothenbach, G. Ye, Thermodynamic modeling of alkali-activated fly ash paste, Cem. Concr. Res. 186 (2024) 107699.

[124] P. Duxson, J.L. Provis, G.C. Lukey, S.W. Mallicoat, W.M. Kriven, J.S. Van Deventer, Understanding the relationship between geopolymer composition, microstructure and mechanical properties, Colloids Surf. A Physicochem. Eng. Asp. 269 (2005) 47–58.

[125] B. Chen, Y. Zuo, S. Zhang, L.M. de Lima Junior, X. Liang, Y. Chen, M.B. van Zijl, G. Ye, Reactivity and leaching potential of municipal solid waste incineration (MSWI) bottom ash as supplementary cementitious material and precursor for alkali-activated materials, Constr. Build. Mater. 409 (2023) 133890.

[126] X. Ke, Y. Duan, Coupling machine learning with thermodynamic modelling to develop a composition-property model for alkali-activated materials, Compos. Part B Eng. 216 (2021) 108801.

[127] B. Sun, G. Ye, G. de Schutter, A review: reaction mechanism and strength of slag and fly ash-based alkali-activated materials, Constr. Build. Mater. 326 (2022) 126843.

[128] Z. Li, Y. Chen, J.L. Provis, Ö. Cizer, G. Ye, Autogenous shrinkage of alkali-activated slag: a critical review, Cem. Concr. Res. 172 (2023) 107244.

[129] A. Wang, Y. Zheng, Z. Zhang, K. Liu, Y. Li, L. Shi, D. Sun, The durability of alkali-activated materials in comparison with ordinary Portland cements and concretes: a review, Engineering 6 (2020) 695–706.

[130] S. Bishnoi, K.L. Scrivener, μic: a new platform for modelling the hydration of cements, Cem. Concr. Res. 39 (2009) 266–274.

[131] Y. Zuo, G. Ye, GeoMicro3D: A Novel Numerical Framework for Simulating the Hydration and Microstructure Formation of Alkali-Activated Materials, in: G, Ye, Proceedings of Workshop on Concrete Modelling and Materials Behaviour in Honor of Professor Klaas van Breugel, RILEM, Delft, The Netherlands, 2018.

[132] Y. Zuo, G. Ye, GeoMicro3D: a novel numerical model for simulating the reaction process and microstructure formation of alkali-activated slag, Cem. Concr. Res. 141 (2021) 106328.

[133] M. Gupta, X. Qiu, M. Omran, Y. Chen, M. Khalifeh, G. Ye, Reaction and microstructure development of one-part geopolymer for wellbore applications – an experimental and numerical study, Cem. Concr. Res. 188 (2025) 107738.

[134] T. Williamson, T. Zhu, J. Han, G. Sant, O.B. Isgor, M.C.G. Juenger, L. Katz, Effect of temperature on N-A-S-(H) and zeolite composition, solubility, and structure, Cem. Concr. Res. 172 (2023) 107213.

[135] P.T. Durdziński, C.F. Dunant, M.B. Haha, K.L. Scrivener, A new quantification method based on SEM-EDS to assess fly ash composition and study the reaction of its individual components in hydrating cement paste, Cem. Concr. Res. 73 (2015) 111–122.

[136] R. Patel, Lattice Boltzmann Method Based Framework for Simulating Physico-Chemical Processes in Heterogeneous Porous Media and its Application to Cement Paste, Ghent University, PhD, 2016.

[137] S. Jiang, J.H. ter Horst, Crystal nucleation rates from probability distributions of induction times, Cryst. Growth Des. 11 (2010) 256–261.

[138] H. Zhang, B. Šavija, E. Schlangen, Combined experimental and numerical study on micro-cube indentation splitting test of cement paste, Eng. Fract. Mech. 199 (2018) 773–786.

[139] X. Li, X. Gu, X. Xia, E. Madenci, X. Chen, Q. Zhang, Effect of water-cement ratio and size on tensile damage in hardened cement paste: insight from peridynamic simulations, Constr. Build. Mater. 356 (2022) 129256.

[140] G. Ye, Percolation of capillary pores in hardening cement pastes, Cem. Concr. Res. 35 (2005) 167–176.
[141] Y. Song, G. Dai, L. Zhao, Z. Bian, P. Li, L. Song, Permeability prediction of hydrated cement paste based on its 3D image analysis, Constr. Build. Mater. 247 (2020) 118527.
[142] C. Liu, M. Zhang, Microstructure-based modelling of chloride diffusivity in non-saturated cement paste accounting for capillary and gel pores, Cem. Concr. Res. 168 (2023) 107153.
[143] J. Zhang, H.-l. Wang, Z.-w. Chen, Q.-f. Liu, X.-y. Sun, J.-j. Zheng, Experimental investigation and numerical simulation for chloride diffusivity of cement paste with elliptical cement particles, Constr. Build. Mater. 337 (2022) 127616.
[144] J.L. Provis, R.J. Myers, C.E. White, V. Rose, J.S.J. van Deventer, X-ray microtomography shows pore structure and tortuosity in alkali-activated binders, Cem. Concr. Res. 42 (2012) 855–864.
[145] S. Das, P. Yang, S.S. Singh, J.C. Mertens, X. Xiao, N. Chawla, N. Neithalath, Effective properties of a fly ash geopolymer: synergistic application of X-ray synchrotron tomography, nanoindentation, and homogenization models, Cem. Concr. Res. 78 (2015) 252–262.
[145] D.P. Bentz, N.S. Martys, A Stokes Permeability Solver for Three-Dimensional Porous Media, US Department of Commerce, Technology Administration, National Institute of Standards and Technology Gaithersburg, MD, USA, 2007.
[147] Z. Xu, Y. Zuo, G. Ye, Lattice Boltzmann simulation of chloride transport in alkali-activated slag, in: G. Ye (Ed.), Webinar, Delft, The Netherlands, 2021.
[148] Q. Ma, S.V. Nanukuttan, P.A.M. Basheer, Y. Bai, C. Yang, Chloride transport and the resulting corrosion of steel bars in alkali activated slag concretes, Mater. Struct. 49 (2016) 3663–3677.
[149] A. Dehghan, K. Peterson, G. Riehm, L. Herzog Bromerchenkel, Application of X-ray microfluorescence for the determination of chloride diffusion coefficients in concrete chloride penetration experiments, Constr. Build. Mater. 148 (2017) 85–95.
[150] R.L. Mitchell, A. Holwell, G. Torelli, J. Provis, K. Selvaranjan, D. Geddes, A. Yorkshire, S. Kearney, Cements and concretes materials characterisation using machine-learning-based reconstruction and 3D quantitative mineralogy via X-ray microscopy, J. Microsc. 294 (2024) 137–145.
[151] P.J. Sánchez, P.J. Blanco, A.E. Huespe, R.A. Feijóo, Failure-oriented multi-scale Variational formulation: Micro-structures with nucleation and evolution of softening bands, Comput. Methods Appl. Mech. Eng. 257 (2013) 221–247.
[152] I.M. Gitman, H. Askes, L.J. Sluys, Coupled-volume multi-scale modelling of quasi-brittle material, Eur. J. Mech. A-Solid 27 (2008) 302–327.
[153] Z. Qian, E. Schlangen, G. Ye, K. van Breugel, Modeling framework for fracture in multiscale cement-based material structures, Materials 10 (2017) 587.
[154] O. Bernard, F.-J. Ulm, E. Lemarchand, A multiscale micromechanics-hydration model for the early-age elastic properties of cement-based materials, Cem. Concr. Res. 33 (2003) 1293–1309.
[155] J. Sanahuja, L. Dormieux, G. Chanvillard, Modelling elasticity of a hydrating cement paste, Cem. Concr. Res. 37 (2007) 1427–1439.
[156] M. Königsberger, B. Pichler, C. Hellmich, Multiscale poro-elasticity of densifying calcium-silicate hydrates in cement paste: an experimentally validated continuum micromechanics approach, Int. J. Eng. Sci. 147 (2020) 103196.
[157] B. Pichler, C. Hellmich, Upscaling quasi-brittle strength of cement paste and mortar: a multi-scale engineering mechanics model, Cem. Concr. Res. 41 (2011) 467–476.
[158] M. Königsberger, M. Hlobil, B. Delsaute, S. Staquet, C. Hellmich, B. Pichler, Hydrate failure in ITZ governs concrete strength: a micro-to-macro validated engineering mechanics model, Cem. Concr. Res. 103 (2018) 77–94.
[159] C. Pichler, R. Lackner, H.A. Mang, A multiscale micromechanics model for the autogenous-shrinkage deformation of early-age cement-based materials, Eng. Fract. Mech. 74 (2007) 34–58.
[160] M. Königsberger, M. Irfan-ul-Hassan, B. Pichler, C. Hellmich, Downscaling based identification of nonaging power-law creep of cement hydrates, J. Eng. Mech. 142 (2016) 04016106.
[161] M. Irfan-ul-Hassan, M. Königsberger, R. Reihsner, C. Hellmich, B. Pichler, How water-aggregate interactions affect concrete creep: multiscale analysis, J. Nanomech. Micromech. 7 (2017) 04017019.
[162] V. Šmilauer, P. Hlaváček, F. Škvára, R. Šulc, L. Kopecký, J. Němeček, Micromechanical multiscale model for alkali activation of fly ash and metakaolin, J. Mater. Sci. 46 (2011) 6545–6555.
[163] M. Königsberger, L. Zelaya-Lainez, O. Lahayne, B.L.A. Pichler, C. Hellmich, Nanoindentation-probed Oliver-Pharr half-spaces in alkali-activated slag-fly ash pastes: multimethod identification of microelasticity and hardness, Mech. Adv. Mater. Struct. 29 (2022) 4878–4889.
[164] G. Fang, M. Zhang, Multiscale micromechanical analysis of alkali-activated fly ash-slag paste, Cem. Concr. Res. 135 (2020) 106141.
[165] R. Caron, R.A. Patel, A. Bogner, F. Dehn, Multi-scale experimental investigation and analytical micro-mechanical modeling to determine Young's modulus of alkali-activated slag concrete, Constr. Build. Mater. 383 (2023) 131272.
[166] Z. Abdollahnejad, M. Mastali, T. Luukkonen, P. Kinnunen, M. Illikainen, Fiber-reinforced one-part alkali-activated slag/ceramic binders, Ceram. Int. 44 (2018) 8963–8976.
[167] S. Nayak, A. Kizilkanat, N. Neithalath, S. Das, Experimental and numerical investigation of fracture behavior of particle-reinforced alkali-activated slag mortars, J. Mater. Civ. Eng. 31 (2019) 04019043.
[168] T.T. Nguyen, H.H. Bui, T.D. Ngo, G.D. Nguyen, M.U. Kreher, F. Darve, A micromechanical investigation for the effects of pore size and its distribution on geopolymer foam concrete under uniaxial compression, Eng. Fract. Mech. 209 (2019) 228–244.
[169] A. Caggiano, I. Peralta, V.D. Fachinotti, G. Goracci, J.S. Dolado, Atomistic simulations, meso-scale analyses and experimental validation of thermal properties in ordinary Portland cement and geopolymer pastes, Comput. Struct. 285 (2023) 107068.